

submitted to Int. J. Mass Spectrom.

Infrared Multiple Photon Dissociation Spectroscopy of Protonated Histidine and 4-Phenyl Imidazole

Murat Citir,^{a,b} Christopher S. Hinton,^a Jos Oomens,^{c,d} Jeffrey D. Steill,^c and P. B. Armentrout^{a,*}^a*Department of Chemistry, University of Utah, Salt Lake City, UT 84112, United States*^b*Abdullah Gül University, Melikgazi / Kayseri, 38039, Turkey*^c*FOM Institute for Plasma Physics "Rijnhuizen", Edisonbaan 14, 3439 MN Nieuwegein, The Netherlands*^d*Van't Hoff Institute for Molecular Sciences, University of Amsterdam, Amsterdam, The Netherlands*

* Corresponding author. Tel.: +1 801 581 7885; fax: +1 801 581 8433.

E-mail address: armentrout@chem.utah.edu (P. B. Armentrout).

Abstract

The gas-phase structures of protonated histidine (His) and the side-chain model, protonated 4-phenyl imidazole (PhIm), are examined by infrared multiple photon dissociation (IRMPD) action spectroscopy utilizing light generated by the free electron laser FELIX. To identify the structures present in the experimental studies, the measured IRMPD spectra are compared to spectra calculated at a B3LYP/6-311+G(d,p) level of theory. Relative energies of various conformers are provided by single point energy calculations carried out at the B3LYP, B3P86, and MP2(full) levels using the 6-311+G(2d,2p) basis set. On the basis of these experiments and calculations, the IRMPD action spectrum for $\text{H}^+(\text{His})$ is characterized by a mixture of $[\text{N}_\pi, \text{N}_\alpha]$ and $[\text{N}_\pi, \text{CO}]$ conformers, with the former dominating. These conformers have the protonated nitrogen atom of imidazole adjacent to the side-chain (N_π) hydrogen bonding to the backbone amino nitrogen (N_α) and to the backbone carbonyl oxygen, respectively. Comparison of the present results to recent IRMPD studies of protonated histamine, the radical $\text{His}^{\bullet+}$ cation, $\text{H}^+(\text{HisArg})$,

$\text{H}_2^{2+}(\text{HisArg})$, and $\text{M}^+(\text{His})$, where $\text{M}^+ = \text{Li}^+, \text{Na}^+, \text{K}^+, \text{Rb}^+, \text{and } \text{Cs}^+$, allows evaluation of the vibrational motions associated with the observed bands.

Keywords: histamine, histidine, imidazole, IRMPD

1. Introduction

Histidine (His) is chemically one of the most flexible protein residues because the imidazole side chain can function as both an acid and base near neutral pH [1]. The histidine molecule presents three potential coordination sites in aqueous solution. The carboxyl group ($\text{pK}_a = 1.9$), the imidazole nitrogen ($\text{pK}_a = 6.1$), and the amino nitrogen ($\text{pK}_a = 9.1$) become available for complexation as pH increases. The acid-base properties of a biomolecule affect physicochemical activities such as solubility, hydrophobicity, and electrostatic interactions that directly impact the biological activity of the molecule in a living system. Because the pK_a of the imidazolium form is around 6, histidine can undergo protonation and deprotonation reactions at physiological pH. Therefore, it functions as a competent proton-transfer mediator in various proteins [2-5]. Histidine also serves as both a hydrogen-bond donor and an acceptor, and this hydrogen-bonding property is of importance in proton-transfer reactions [5] and in organizing the active centers of enzymes. As a consequence, histidine is often found at the catalytic sites of protein enzymes.

In recent years, the structures of many proteins have been studied by X-ray crystallography; however, because of the poor sensitivity of X-ray crystallography in detecting hydrogen atoms, the protonation structures and hydrogen-bonding interactions of amino acid side chains are not well resolved in many cases. To obtain such information, vibrational spectroscopy is a powerful method as it is more sensitive to chemical bonds and molecular interactions. In the case of histidine, its protonation state, metal binding, and hydrogen bonding interactions have been investigated using both Raman [6-18] and Fourier transform infrared (FTIR) [19] spectroscopy. Huang et al. [20] investigated the neutral, protonated, and deprotonated histidine

conformers in the gas phase using time-dependent density functional theory (TDDFT) to calculate the electronic spectra and charge-transfer processes. Also, Hasegawa et al. [21] studied 4-methylimidazole (a simple model compound of the histidine side chain) and its different protonation forms using FTIR and Raman spectra for systematic investigation of vibrational markers of the protonation state of histidine.

Infrared multiple photon dissociation (IRMPD) spectroscopy has been used to probe the structures of ionized complexes in the gas phase and can be a powerful tool for understanding ion–protein interactions. An important advantage of this technique is the ability to investigate the structures of biomolecules in isolation, where complicating structural effects of solvent and counter-ions are absent. Recently, gas-phase structures of protonated histamine [22], histidine radical cation ($\text{His}^{\bullet+}$) [23], $\text{H}^+(\text{HisArg})$ and $\text{H}_2^{2+}(\text{HisArg})$ [24], and $\text{M}^+(\text{His})$ [25], where $\text{M}^+ = \text{Li}^+, \text{Na}^+, \text{K}^+, \text{Rb}^+, \text{and } \text{Cs}^+$, have all been investigated by IRMPD spectroscopy utilizing light generated by a free electron laser. In the present study, we measure the IRMPD action spectra for photodissociation of protonated His and 4-phenyl imidazole (PhIm), where the latter provides a model for assessing the vibrations of the imidazole side-chain ring. Conformations of these molecules are identified by comparing the experimental spectra to IR spectra of the low-lying structures of the cationized His and PhIm complexes predicted by quantum chemical calculations at the B3LYP/6-311+G(d,p) level of theory. IRMPD action spectra for $\text{H}^+(\text{His})$ and $\text{H}^+(\text{PhIm})$ are also compared to the previous results for $\text{H}^+(\text{histamine})$, $\text{His}^{\bullet+}$, $\text{H}^+(\text{HisArg})$, $\text{H}_2^{2+}(\text{HisArg})$, and $\text{M}^+(\text{His})$, where $\text{M}^+ = \text{Li}^+, \text{Na}^+, \text{K}^+, \text{Rb}^+, \text{and } \text{Cs}^+$.

2. Experimental and Computational Section

2.1. Mass Spectrometry and Photodissociation

Experiments were performed using the Free Electron Laser for Infrared eXperiments (FELIX) [26] in combination with a home-built Fourier transform ion cyclotron resonance (FTICR) mass spectrometer, which has been described in detail elsewhere [27-29]. Protonated histidine and protonated phenyl imidazole complexes were generated using a Z-spray

(Micromass UK Ltd.) electrospray ionization source. Solutions used were 1.0 – 3.0 mM His with 1 mM acetic acid in 50% MeOH and 50% H₂O for H⁺(His) and 1.0 mM phenyl imidazole acidified with acetic acid in 58% MeOH and 42% H₂O for H⁺(PhIm). Solution flow rates were about 10 μ L/min and the electrospray needle was held at a voltage of \sim 3.2 kV. Ions were accumulated in a hexapole trap for about 4 s followed by pulsed extraction through a quadrupole bender prior to being injected into the ICR cell via a radio frequency (rf) octopole ion guide. Electrostatic pulsing of the dc bias of the ion transfer octopole allows ions to be captured in the ICR cell without the use of a gas pulse [28]. In contrast to the conventional gas pulsing method to stop the ions, this technique does not cause collisional heating of the ions. The precursor ions were mass selected using stored waveform inverse Fourier transform (SWIFT) techniques and irradiated by the FEL at pulse energies of 50 mJ per macropulse of 5 μ s duration, although they fell off to about 20 mJ toward the blue edge of the scan range. Complexes were irradiated for 2 - 4 s, corresponding to interaction with 10 - 20 macropulses. The fwhm bandwidth of the laser was typically 0.5% of the central wavelength. For the present experiments, spectra were recorded over the wavelength range 19.4 μ m (520 cm⁻¹) to 5.5 μ m (1820 cm⁻¹), which can be covered with a single setting of the electron beam energy of FELIX.

2.2. Computational Details

Our protocol for finding all low-lying conformations of metal cation-amino acid complexes has been described elsewhere [30]. To find the global energy minimum and all low-energy geometries, a large number of possible conformations were screened using a simulated annealing methodology with the AMBER program and the AMBER force field based on molecular mechanics [31]. All possible structures identified this way were subsequently optimized using NWChem [32] at the HF/3-21G level [33,34]. Unique structures for each system were optimized using Gaussian 09 [35] at the B3LYP/6-31G(d) level of theory [36,37] with the “loose” keyword (maximum step size 0.01 au and an RMS force of 0.0017 au) to facilitate convergence. Unique structures obtained from this procedure were then chosen for

higher-level geometry optimization and frequency calculations using DFT at the B3LYP/6-311+G(d,p) level of theory [38]. Single point energy calculations were carried out at the B3LYP, B3P86, and MP2(full) levels using the 6-311+G(2d,2p) basis set [38]. Zero-point vibrational energy (ZPE) corrections were determined using vibrational frequencies calculated at the B3LYP/6-311+G(d,p) level scaled by a factor of 0.989 [39]. Relative energies at 0 K are converted to 298 K free energies using the rigid rotor/harmonic oscillator approximation with rotational constants and vibrational frequencies calculated at the B3LYP/6-311+G(d,p) level. As will be seen below, the relative ΔG_{298} excitation energies are comparable to the analogous differences in the ΔH_0 values.

Vibrational frequencies and intensities were calculated using the harmonic oscillator approximation and analytical derivatives of the energy-minimized Hessian at the B3LYP/6-311+G(d,p) level of theory. Each of the resulting structures was found to have all real harmonic vibrational frequencies at this level of theory indicating that they are local minima on the potential energy surface. For comparison to IRMPD spectra, frequencies were scaled by 0.975 as this scaling factor leads to good agreement between calculated and experimentally well-resolved peaks and is in accord with previous IRMPD studies of amino acid complexes in this spectral region as well [40-45]. Calculated vibrational frequencies are broadened using a 20 cm^{-1} fwhm Gaussian line shape for comparison with experimental spectra.

At the request of a reviewer, we also calculated geometries and single point energies adding a diffuse function for hydrogen, i.e., R/6-311++G(2d,2p)//B3LYP/6-311++G(d,p), where R indicates B3LYP, B3P86, and MP2(full) levels. This is intended to provide a better description of hydrogen bonding, even though previous explorations in our group have indicated that hydrogen diffuse functions have negligible effects on geometries and relative energies [46-49]. In the present case, six conformers of three different types were examined. Structures were essentially unchanged with hydrogen bonds (a total of 16 interactions) changing by -0.0025 to $+0.0008\text{ \AA}$, with the average absolute change being $0.0006 \pm 0.0007\text{ \AA}$. Relative energies at this level of theory agreed with those presented below within 0.1 kJ/mol in all cases. Furthermore,

vibrational frequencies are the same within 0.01%. Because the addition of diffuse functions to the hydrogen atoms introduces little distortions, energy changes, or vibrational shifts, such calculations were not pursued further for any other conformations.

3. Results and Discussion

3.1. IRMPD Action Spectroscopy

The photodissociation spectra of protonated (m/z 156) His both as depletion of the parent ion and the yield for loss of $\text{H}_2\text{O} + \text{CO}$ (m/z 110) (corrected for laser power and uncorrected) are shown in Figure S1 of the Supporting Information. Very small amounts (> 10 times smaller) of just H_2O loss were also detected. These decomposition pathways match the lowest energy products observed in the collision-induced dissociation (CID) spectrum of $\text{H}^+(\text{His})$, as observed previously [50,51]. Parent and product ion intensities were monitored as a function of the laser frequency, and the IRMPD yield shown in Figure S1 and the figures below was calculated as the integrated intensity ratio $I_{110} / (I_{110} + I_{156})$. This was normalized linearly with laser power to roughly account for the change in laser power as a function of photon energy. As shown in Figure S1, the depletion spectrum of the m/z 156 parent ion is similar to the appearance spectrum of the m/z 110 product ion. The depletion of the parent ion signal exceeds 50% at the most intense resonances. Because the IRMPD yield is normalized for parent ion fluctuations, it exhibits better signal-to-noise ratio than the depletion signal and will be compared to the calculated spectra.

To provide a spectrum characteristic of the imidazole (Im) side-chain of His, we also tried acquiring the IRMPD spectrum of protonated Im. Unfortunately, this molecule is sufficiently small that dissociation is inefficient and no spectrum could be collected. To overcome this size limitation, it would be useful to examine Im substituted at the 4-position to mimic the His side-chain. Simple alkyl-substituted Im are unstable or not readily available, but 4-phenyl imidazole (PhIm) is commercially available. For protonated PhIm, two IR photodissociation pathways were observed corresponding to the loss of HCN (m/z 118) and 2

HCN (m/z 91). The sum of these two decomposition pathways is shown as the IRMPD action spectrum below.

3.2. Theoretical Results (Structures)

The nomenclature used here to identify different structural isomers of $H^+(\text{His})$ is similar to that described previously for the IRMPD study of $M^+(\text{His})$ [25]; however, here the atoms of His are named according to the IUPAC Compendium of Chemical Terminology (Gold Book), in which positions of the nitrogen atoms of the imidazole ring relative to the side chain are denoted by *pros* ('near', abbreviated π and also referred to as N_1) and *tele* ('far', abbreviated τ or N_3) [52], Figure 1. In addition, conformations of protonated His are identified by their proton binding sites in brackets, followed by a description of the histidine orientation, named by a series of dihedral angles starting from the carboxylic acid hydrogen of the backbone and going to the imidazole side-chain nitrogen (N_π) ($\angle\text{HOCC}$, $\angle\text{OCCC}$, $\angle\text{CCCC}$, and $\angle\text{CCCN}_\pi$, respectively). Dihedral angles are distinguished as *cis* (c, for angles between $0^\circ - 45^\circ$), *gauche* (g, $45^\circ - 135^\circ$), or *trans* (t, $135^\circ - 180^\circ$), and + or - indicating their sign when necessary to distinguish similar structures. In some cases, these four dihedral angles are insufficient to distinguish similar conformers and a fifth dihedral angle is added in parentheses to define the electron lone pair orientation of the $N_\alpha\text{H}_2$ group. In most conformations, this orientation is *cis* with respect to the adjacent backbone CC bond, such that only alternate orientations (*gauche* or *trans*) are indicated by this fifth dihedral angle.

Eight low-lying and representative higher energy conformations of $H^+(\text{His})$ are illustrated in Figure 1, with a total of 24 structures shown in Figure S2 in the Supporting Information. The protonated histidine complex, $H^+(\text{His})$, has a set of low energy structures, $[N_\pi, N_\alpha]$, in which the protonated imidazole side-chain hydrogen bonds to the backbone amino nitrogen ($N_\pi\text{H}\cdots N_\alpha$), Figure 1. If the proton shifts to N_α , retaining a hydrogen bond to N_π , the $[N_\alpha, N_\pi]$ conformer is formed. These structures are not shown in Figure 1 as the only significant distinction from the analogous $[N_\pi, N_\alpha]$ structures is the position of the bridging proton. Other possible binding

motifs are $[N_\pi, CO]$ and $[N_\pi, OH]$, in which the protonated imidazole side-chain hydrogen bonds to the backbone carbonyl oxygen ($N_\pi H \cdots OC$) or hydroxyl oxygen ($N_\pi H \cdots OH$). The latter are not shown in Figure 1 because they resemble the $[N_\pi, CO]$ structures with the carboxylic group rotated by 180° . Relative Gibbs free energies at 298 K and relative energies at 0 K including zero-point energy (ZPE) corrections with respect to the ground state calculated at three different levels of theory are given in Table 1 for $H^+(\text{His})$. Because the relative Gibbs free energies may be more relevant in describing the experimental distributions, these values are used throughout the discussion below.

At all levels of theory, the ground state (GS) structure for $H^+(\text{His})$ is $[N_\pi, N_\alpha]$ -tggc, Figure 1. In addition, there are five other stable geometries having this binding motif. Only slightly higher in energy, 1 – 5 kJ/mol, is the tgtc conformer. Both the tggc and tgtc structures have similar $N_\pi H \cdots N_\alpha$ hydrogen bond lengths (1.916 and 1.902 Å, respectively), but the former appears to be stabilized by a stronger $N_\alpha H \cdots OC$ interaction, as suggested by bond lengths of 2.272 and 2.420 Å, respectively. $[N_\pi, N_\alpha]$ -ttgc and ttgc conformers are found at slightly higher energies, 4 – 5 and 5 – 10 kJ/mol above the GS, respectively, and have slightly longer $N_\pi H \cdots N_\alpha$ hydrogen bond lengths (1.967 and 1.932 Å, respectively). These conformers differ from the lower energy structures by the $\angle OCCC$ dihedral being trans rather than gauche, which rotates the carboxylic acid such that the $N_\alpha H \cdots OC$ hydrogen bond is replaced by a weaker $N_\alpha H \cdots OH$ hydrogen bond, Figure 1. Finally, the cggc and cgtc conformers have geometries similar to the tggc and tgtc structures, but the hydroxyl hydrogen is rotated such that it no longer interacts with the carbonyl oxygen, Figure S2, which costs about 31 and 34 kJ/mol, respectively. These conformers have $N_\pi H \cdots N_\alpha$ hydrogen bond lengths of 1.966 and 1.903 Å, respectively. Similar comparisons hold for the six analogous $[N_\alpha, N_\pi]$ conformers, shown in Figure S2. At the B3LYP and B3P86 levels, all $[N_\alpha, N_\pi]$ conformers lie higher in energy than their $[N_\pi, N_\alpha]$ counterparts, with the $[N_\alpha, N_\pi]$ -tgtc variant being lowest in energy. In contrast, MP2 calculations find that the $[N_\alpha, N_\pi]$ -tggc and cgtc conformers are slightly lower in energy than their $[N_\pi, N_\alpha]$ analogues, with the tggc conformer being lowest of the $[N_\alpha, N_\pi]$ conformers. The $[N_\alpha, N_\pi]$ conformers have

relatively short $N_\alpha H \cdots N_\pi$ hydrogen bond lengths of 1.63 – 1.66 Å, indicating that the proton generally prefers to be on the N_π nitrogen.

Eight different $[N_\pi, CO]$ conformers were located with the ctg_+g_- structure being the lowest at the DFT levels of theory, 2 – 4 kJ/mol above the GS. This structure has the shortest $N_\pi H \cdots OC$ hydrogen bond length (1.673 Å) among the $[N_\pi, CO]$ conformers and is stabilized by a $OH \cdots N_\alpha$ hydrogen bond, Figure 1. The next four conformers in energy are all $ttgg$ with $N_\pi H \cdots OC$ hydrogen bond lengths of 1.78 – 1.83 Å, Figures 1 and S2. In these conformers, the hydroxyl group has rotated, losing the $OH \cdots N_\alpha$ hydrogen bond and replacing it with an $OH \cdots OC$ interaction augmented by various $N_\alpha H \cdots O(H)$ interactions depending on the orientation of the $N_\alpha H_2$ group, (g) or (t). DFT calculations find that these species lie 5 – 11 kJ/mol above the GS and 1 – 9 kJ/mol above the $[N_\pi, CO]-ctg_+g_-$ structure, whereas MP2 calculations find that the lowest energy $[N_\pi, CO]$ conformer is $ttg_-g_+(t)$ with the ctg_+g_- variant lying 5 kJ/mol higher. Finally, there are three higher lying conformers, ctg_-g_+ , $ctg_-g_+(t)$, and $cggg$, having $N_\pi H \cdots OC$ hydrogen bond lengths of 1.74 – 1.85 Å, Figure S2. The lowest of these, ctg_-g_+ , is stabilized by a $OH \cdots N_\alpha$ hydrogen bond such that it lies 10 – 15 kJ/mol above ctg_+g_- . The other two lie 21 – 30 kJ above ctg_+g_- . Four $[N_\pi, OH]$ conformers have structures similar to the analogous $ttgg$ geometries shown in Figure 1, with the carboxylic acid group rotated by about 180°. These species lie fairly high in energy, 23 – 38 kJ/mol above the GS conformer and 15 – 31 kJ/mol above analogous $[N_\pi, CO]$ conformers, Table 1.

We also carefully examined the proton transfer process that connects the $[N_\pi, N_\alpha]$ and $[N_\alpha, N_\pi]$ conformers, locating the transition state (TS) for all six side-chain orientations, Table 1. B3LYP, B3P86, and MP2(full) level calculations reveal that the barriers ($N_\pi \rightarrow TS$) are 6 – 13, 0 – 6, and 2 – 9 kJ/mol, respectively. At the B3LYP level, except for $tgtc$ and $cgtc$, the 298 K free energies of these TSs lie *below* that for the associated $[N_\alpha, N_\pi]$ conformer, indicating that the latter collapse with no energy barrier to the analogous $[N_\pi, N_\alpha]$ form. At the B3P86 level, all six $[N_\alpha, N_\pi]$ conformers collapse to the $[N_\pi, N_\alpha]$ forms, whereas MP2(full) theory suggests that only the $[N_\alpha, N_\pi]-ttgc$ conformer will collapse. Similar trends are found for the 0 K enthalpies.

Figure 2 shows the potential energy surfaces along the N_π -H- N_α coordinate linking all six $[N_\pi, N_\alpha]$ and $[N_\alpha, N_\pi]$ conformers calculated at the B3LYP/6-311+G(d,p) level by explicitly controlling the N_π -H bond distance and allowing all other degrees of freedom to optimize. For comparison, the potential for protonated histamine, which is His without the carboxylic acid on the α -carbon, is also included. It can be seen that in all cases two separate minima in an asymmetric double-well potential exist. Therefore the relative stabilities and instabilities noted above are the result of differences in zero point energies. This is partially indicated by the zero of the scale in Figure 2, which is set to the zero point energy of the harmonically calculated proton motion of the $[N_\pi, N_\alpha]$ conformers (scaled frequencies ranging from 3025 – 3170 cm^{-1}). Anharmonic frequency calculations for the $[N_\pi, N_\alpha]$ -tggc conformer find a modest shift from 3085 cm^{-1} (harmonic, 0.975 scaling) to 2937 cm^{-1} (anharmonic, unscaled). Despite this, use of harmonic frequencies on such an anharmonic potential is not exact and use of the harmonic frequency for proton motion of the $[N_\alpha, N_\pi]$ conformers would place the zero differently for each conformer. These frequencies range from 2338 – 2465 cm^{-1} (scaled), which places the zero point level for these conformers roughly 14 kJ/mol above the bottom of the $[N_\alpha, N_\pi]$ potential wells.

3.3. Comparison of experimental and theoretical IR spectra: $H^+(\text{His})$

The power-corrected experimental spectrum for $H^+(\text{His})$ is shown in Figure 3 and exhibits major peaks at 1778, 1609, 1399, 1306, 1132, 822, 676, and 609 cm^{-1} . Additional weaker bands are observed at 1747, 1433, 1340, ~990, ~923, and ~742 cm^{-1} , with an unresolved shoulder at 1079 cm^{-1} . Figure 3 compares the experimental spectrum with those calculated for the most stable conformers of $[N_\pi, N_\alpha]$, $[N_\alpha, N_\pi]$, and $[N_\pi, \text{CO}]$, which are the most likely conformers to be populated along with $[N_\pi, N_\alpha]$ -tgtc (and possibly tgc) on the basis of the theoretical 298 K free energies, Table 1. Figure S3 shows the predicted spectra of all conformations for comparison, and Table 2 makes qualitative assignments of bands predicted for the $[N_\pi, N_\alpha]$ -tggc and $[N_\pi, \text{CO}]$ -ctg₊g₋ conformers on the basis of visualizing the molecular motions. Figure S3 shows that the four lowest structures for $[N_\pi, N_\alpha]$, all txxc where x = g or t,

have similar spectra, as do the four analogous structures for $[N_\alpha, N_\pi]$. In contrast, the *cis* orientation of $\angle\text{HOCC}$ in the higher-energy *cxgc* conformers of both $[N_\pi, N_\alpha]$ and $[N_\alpha, N_\pi]$ removes the $\text{OH}\cdots\text{OC}$ interaction such that the intense bands associated with the C-OH stretch and COH bend motions shift from ~ 1140 to $\sim 1240\text{ cm}^{-1}$ and those for the CO stretch shift from ~ 1780 to $\sim 1800\text{ cm}^{-1}$. The four $[N_\pi, \text{CO}]\text{-cxgg}$ conformers show similar spectra although the intense band associated with the C-OH stretch and COH bend motions is located at $\sim 1380\text{ cm}^{-1}$ (shifted because of the $\text{OH}\cdots\text{N}_\alpha$ interaction) for *ctg₊g₋* and *ctg₋g₊* and at $\sim 1290\text{ cm}^{-1}$ for *ctg₊g₊(t)* and *cggg*, which no longer have the $\text{OH}\cdots\text{N}_\alpha$ interaction. In these four cases, the CO stretch is red-shifted to $\sim 1745\text{ cm}^{-1}$. In the four $[N_\pi, \text{CO}]\text{-ttgg}$ conformers, which are all similar, the CO stretch is red-shifted even further, to $1705 - 1730\text{ cm}^{-1}$, and the C-OH stretch and COH bend returns to $\sim 1160\text{ cm}^{-1}$. The four $[N_\pi, \text{OH}]\text{-txgg}$ conformers are similar to the $[N_\pi, \text{CO}]\text{-ttgg}$ analogues except the CO stretch has shifted up to $\sim 1800\text{ cm}^{-1}$.

The comparison in Figure 3 shows that the experimental spectrum is generally consistent with that predicted for the lowest-energy conformer, $[N_\pi, N_\alpha]\text{-tggc}$, Table 1. The principal disagreements are the lack of predicted bands at 1747 and 1340 cm^{-1} . Relative intensities are not reproduced particularly well, with predicted bands between 900 and 1000 cm^{-1} being too strong and that for the band at 1132 cm^{-1} being too weak. If the predicted bands at 1107 and 1139 cm^{-1} were closer together, as they are for the $[N_\pi, N_\alpha]\text{-tgtc}$ and *ttgc* conformers, Figure S3, the agreement would improve. The carbonyl stretch in the observed spectrum at 1778 cm^{-1} is reproduced well by the $[N_\pi, N_\alpha]\text{-tggc}$ spectrum (1775 cm^{-1}), although the predicted intensity is too large. The weak bands observed are generally more delocalized bends and stretches, Table 2, but they are reproduced quite well by the $[N_\pi, N_\alpha]$ calculated spectra. The peak at 1747 cm^{-1} cannot be explained by any of the $[N_\pi, N_\alpha]$ or $[N_\alpha, N_\pi]$ conformers but is consistent with the predicted $[N_\pi, \text{CO}]\text{-cxgg}$ spectra. For example, the low-lying $[N_\pi, \text{CO}]\text{-ctg₊g₋}$ structure exhibits a red-shifted carbonyl stretch at 1736 cm^{-1} . The shift occurs because this structure forms a hydrogen bond between the protonated imidazole side-chain nitrogen (N_π) and the backbone carbonyl, whereas a weaker $\text{N}_\alpha\text{H}\cdots\text{OC}$ hydrogen bond is present in the $[N_\pi, N_\alpha]$ and $[N_\alpha, N_\pi]$

conformers, Figure 1. The remainder of the bands predicted for $[N_\pi, CO]\text{-ctg}_+\text{g}_-$ fall at similar positions to those of $[N_\pi, N_\alpha]\text{-tggc}$, such that its presence is consistent with the experimental spectrum. One exception is a band at 882 cm^{-1} , where some intensity in the experimental spectrum can also be observed. We also note that the extremely intense band at 1387 cm^{-1} in the $[N_\pi, CO]\text{-ctg}_+\text{g}_-$ spectrum, which corresponds to a COH bend and C-OH stretching motion, shifts to 1342 cm^{-1} when an anharmonic frequency calculation is performed, potentially explaining the unassigned band observed at 1340 cm^{-1} . The results of the anharmonic frequency calculation is shown for all the bands in this frequency range in Figure S4, along with a comparable calculation for the $[N_\pi, N_\alpha]\text{-tggc}$ conformer. Few bands shift appreciably between the scaled harmonic and unscaled anharmonic calculation, so the comparison shown in Figure 3 remains reasonable.

Although much of the spectrum shown for the $[N_\alpha, N_\pi]\text{-tggc}$ conformer can agree with the experimental spectrum, Figure 3, there is little if any intensity observed near 1500 cm^{-1} , where the predicted spectra for all six $[N_\alpha, N_\pi]$ conformers have intense bands associated with the umbrella motion of the $N_\alpha\text{H}_3$ group. Likewise, there is no evidence in the experimental spectrum for a carbonyl stretch near 1800 cm^{-1} , suggesting that the $[N_\pi, N_\alpha]\text{-cgxc}$, $[N_\alpha, N_\pi]\text{-cgxc}$, and $[N_\pi, OH]$ conformers are not present experimentally. Both conclusions are generally consistent with the relative energetics of these species, Table 1.

On the basis of calculated spectra and thermodynamic data, $[N_\pi, N_\alpha]\text{-txxc}$ conformers are identified as the major carrier of the measured IRMPD spectrum with total predicted populations of 68 – 75% and the tggc and tgtc conformers accounting for most of this intensity. $[N_\pi, CO]$ conformers are predicted to account for 3 – 20%, consistent with the observation of the peak at 1747 cm^{-1} and perhaps that at 1340 cm^{-1} . MP2 theory suggests that the $[N_\alpha, N_\pi]$ conformers have a population of 29%, whereas the DFT calculations put this below 3%. The latter prediction seems more in line with the experimental observations, although the complex coupling between the potential wells associated with these conformations seen in Figure 2 may complicate this conclusion.

3.4. Comparison of experimental and theoretical IR spectra: H^+ (4-phenyl imidazole)

Figure 4 shows the experimental IRMPD action spectra of H^+ (PhIm) and H^+ (His) compared with calculated IR spectra for lowest energy conformer of H^+ (PhIm). This structure has the proton on the imidazole nitrogen with the two rings twisted out of planarity by 35° , Figure 4. Clearly, protonation anywhere else will be much higher in energy and the rigidity of the phenyl side-chain restricts the number of possible structures. The predicted spectrum for H^+ (PhIm) shows a close correspondence to the observed spectrum, in terms of both band positions and relative intensities. The primary exception is the band at 1340 cm^{-1} , which is not predicted accurately, either because the band predicted at 1281 cm^{-1} is shifted or the band at 1326 cm^{-1} should be more intense. (An anharmonic frequency calculation for H^+ (PhIm) is very similar to the scaled harmonic spectrum in Figure 4, with no large shifts in any band having noticeable intensity.) Notably, the band at 1340 cm^{-1} in the H^+ (His) spectrum was also not accurately reproduced, a comparison that might suggest that this corresponds to a motion of the imidazole side chain (in contrast to the assignment based on the anharmonic frequency calculation). Given these provisos, the experimental IRMPD action spectrum can be explained adequately by the calculated spectrum of the ground state conformer.

Detailed analysis of band positions and vibrational assignments for H^+ (PhIm) are given in Table 3 on the basis of visualizing the molecular motions. Although the majority of the bands in the IRMPD spectrum of H^+ (PhIm) correspond to motions throughout the molecule, the most intense bands generally involve vibrations of the imidazole ring. Only the band at 752 cm^{-1} is primarily centered in the phenyl ring, an out-of-plane CH bend. Given the non-polar nature of the phenyl ring, this seems reasonable.

Comparison of the H^+ (PhIm) spectrum with that of H^+ (His) shows many similar features, Figure 4. Obvious differences are that H^+ (PhIm) no longer exhibits the carbonyl stretches at $1750 - 1800\text{ cm}^{-1}$ nor the band at 1139 cm^{-1} corresponding to the COH bend and C-OH stretch, which gives much of the intensity to the 1132 cm^{-1} peak in the H^+ (His) spectrum. Likewise, the band at about 700 cm^{-1} in H^+ (PhIm) is enhanced by contributions from the phenyl group. One

interesting difference in the two spectra is the apparent shift in the bands at 1399 and 1433 cm^{-1} for $\text{H}^+(\text{His})$ to 1448 and 1482 cm^{-1} for $\text{H}^+(\text{PhIm})$. Actually, the predicted band positions between the two molecules do not change appreciably in this region, but intensities vary because some modes gain in intensity by interactions with the polar amino acid group in His. For example, the band at 1399 cm^{-1} for $\text{H}^+(\text{His})$, which corresponds mainly to an in-plane N_πH bend, is not observed for $\text{H}^+(\text{PhIm})$ because its predicted intensity has dropped by a factor of 33. Overall, this comparison demonstrates the contributions that the imidazole side-chain make to the spectrum of $\text{H}^+(\text{His})$.

3.5. Comparison of experimental IR spectra: $\text{H}^+(\text{His})$ versus $\text{H}^+(\text{histamine})$

In a recent study, Lagutschenkov et al. [22] published a detailed analysis of the IRMPD spectrum of protonated histamine, a neurotransmitter, which is His without the carboxylic acid on the α -carbon. They compared the experimental IRMPD spectrum of protonated histamine with predicted IR spectra of several low-energy structures, which were characterized by quantum-chemical calculations at the B3LYP and MP2 levels of theory using the cc-pVDZ basis set. These calculations predict the most stable conformer is the imidazolium-type conformer with protonation at the imidazole ring and gauche conformation of the ethylamine side chain, which is significantly stabilized by an intramolecular ionic $\text{N}_\pi\text{H}\cdots\text{N}_\alpha$ hydrogen bond. This structure is equivalent to the $[\text{N}_\pi, \text{N}_\alpha]$ conformers for $\text{H}^+(\text{His})$, Figure 1, which are all the same once H replaces the COOH group. Close in energy is the gauche ammonium-type N_α tautomer, equivalent to $[\text{N}_\alpha, \text{N}_\pi]$ conformers of $\text{H}^+(\text{His})$. All other conformations found for $\text{H}^+(\text{histamine})$ no longer contain the $\text{N}_\pi\cdots\text{H}\cdots\text{N}_\alpha$ hydrogen bond and are therefore much higher in energy (> 32 kJ/mol). Similar to the findings discussed above for the analogous $\text{H}^+(\text{His})$ complexes, B3LYP calculations prefer $\text{H}^+(\text{histamine})$ $[\text{N}_\pi, \text{N}_\alpha]$, the imidazolium ion structure, by 6.3 kJ/mol, whereas MP2 calculations stabilize the $[\text{N}_\alpha, \text{N}_\pi]$, the ammonium ion structure, actually finding that it lies lower in energy by 1.7 kJ/mol. Larger basis sets shift the balance back to the $[\text{N}_\pi, \text{N}_\alpha]$ structure, with the relative differences between B3LYP and MP2 remaining. These results are confirmed

here where, for the three levels of theory used above, the $[N_\pi, N_\alpha]$ -type is the ground state by 7.8 (B3LYP), 5.2 (B3P86), and -0.1 (MP2) kJ/mol, respectively.

Good agreement was found between and the experimental spectrum and the predicted spectrum for $H^+(\text{histamine})$ $[N_\pi, N_\alpha]$, whereas the $[N_\alpha, N_\pi]$ structure was concluded to contribute only a minor amount to the observed spectrum. Interestingly, as Lagutschenkov et al. point out, all other related protonated neurotransmitter ions studied to date prefer protonation at the alkylamino side chain, such that histamine is unique in its preference for imidazole protonation.

The IRMPD action spectra of $H^+(\text{His})$ and $H^+(\text{histamine})$ have many similar features. Bands at 1609, 1433, 1399, 1340, 1306, 1132, 1079, ~990, ~923, 822, 798, 676, and 609 cm^{-1} in the spectrum of $H^+(\text{His})$ are observed at 1598, 1453, 1389, 1359, 1293, 1107, 1075, 997, 909, 830, 788, 685, and 607 cm^{-1} in the protonated histamine spectrum. This can be seen by a comparison of the B3LYP/6-311+G(d,p) calculated spectra in Figure 5. Carbonyl stretches (1778 and 1747 cm^{-1}) and the OCO bend (742 cm^{-1}) in the $H^+(\text{His})$ spectrum are not observed for protonated histamine for obvious reasons. Likewise, the COH bend and C-OH stretch contributes to the experimental band in $H^+(\text{His})$ at 1132 cm^{-1} , thereby blue shifting it from the 1107 cm^{-1} observed for $H^+(\text{histamine})$, assigned to mainly an in-plane $N_\pi\text{H}$ bend. Overall, this comparison is consistent with the assignment above, namely, that the $[N_\pi, N_\alpha]$ form of $H^+(\text{His})$ dominates the experimental spectrum, with additional contributions from the $[N_\pi, \text{CO}]$ form, which is not available to $H^+(\text{histamine})$.

In making this comparison, we did note one interesting anomaly in comparing IR spectra for the most stable conformer of $H^+(\text{histamine})$ calculated at the B3LYP/6-311+G(d,p) level compared with that reported by Lagutschenkov et al. [22]. They agree well over the experimental range examined in most respects, with average deviations between band positions of $6 \pm 6 \text{ cm}^{-1}$ except for the band associated with the out-of-plane $N_\pi\text{H}$ bend, i.e., a proton motion perpendicular to the $N_\pi\text{-H}^+\cdots\text{N}_\alpha$ hydrogen bond. Here, our predicted frequency (1016 cm^{-1} , 0.975 scaling) differs by 62 cm^{-1} (after scaling,) with that for the B3LYP/cc-pVDZ calculations (1078 cm^{-1} , 0.98 scaling), where the latter agree better with experiment (1075 cm^{-1}).

This difference appears to be exclusively one related to the size of the basis set as B3LYP/aug-cc-pVDZ, B3LYP/cc-pVTZ, and B3LYP/aug-cc-pVTZ calculations yield frequencies for this motion of 1036, 1026, and 1018 cm^{-1} (0.98 scaling); however, this frequency is nearly unique in this regard. For example, the in-plane bend of the same N_πH has calculated frequencies of 1117, 1114, 1121, 1118 (0.98 scaling), and 1113 cm^{-1} (0.975 scaling) for cc-pVDZ, aug-cc-pVDZ, cc-pVTZ, aug-cc-pVTZ, and 6-311+G(d,p) basis sets. All other frequencies in the experimental range of interest agree with one another with similarly small variations.

3.6. Comparison of experimental IR spectra: $\text{H}^+(\text{His})$ and $\text{His}^{\bullet+}$

Recently, Steill et al. [23] used IRMPD spectroscopy to study the histidine radical cation. They compared the experimental IRMPD spectrum of $\text{His}^{\bullet+}$ with predicted IR spectra of several low energy structures, finding a good match with the predicted IR spectrum of the global minimum structure, a captodative radical ion that has a structure essentially the same as $[\text{N}_\pi, \text{CO}]\text{-ttg}_+\text{g}_-(\text{t})$ shown in Figure 1 but without the hydrogen atom on the α -carbon. Notably this radical center allows the $\text{H}_2\text{N-C-COOH}$ atoms to be nearly coplanar, allowing resonant stabilization along the NCCO atoms and a shorter $\text{N}_\pi\text{H}\cdots\text{OC}$ hydrogen bond, 1.68 Å compared to 1.78 Å for $[\text{N}_\pi, \text{CO}]\text{-ttg}_+\text{g}_-(\text{t})$ as calculated at the B3LYP/6-311+G(d,p) level. The IRMPD action spectra of $\text{H}^+(\text{His})$ and $\text{His}^{\bullet+}$ have many similar features. Bands comparable to those at 1609, 1399, 1132, 822, 742, 676, and 609 cm^{-1} in the spectrum of $\text{H}^+(\text{His})$ are also observed in the $\text{His}^{\bullet+}$ spectrum. Key differences in the spectra are shifts in the observed carbonyl stretches for $\text{H}^+(\text{His})$ at 1778 and 1747 cm^{-1} to 1666 cm^{-1} for $\text{His}^{\bullet+}$, and the presence of a band at about 1490 cm^{-1} for $\text{His}^{\bullet+}$, which corresponds to stretches along the $\text{N}_\alpha\text{C}_\alpha\text{CO}$ backbone. The latter band clearly shifts because of the resonant delocalization associated with the radical center. Comparison of the $[\text{N}_\pi, \text{N}_\alpha]$ and $[\text{N}_\pi, \text{CO}]$ spectra of Figure 3 also shows a red shift in the carbonyl stretch resulting from the stronger $\text{N}_\pi\text{H}\cdots\text{OC}$ hydrogen bond in the latter structure (and $\text{His}^{\bullet+}$), but not as large a shift as for $\text{His}^{\bullet+}$. This demonstrates that the resonant delocalization

from the C_{α} radical center of $\text{His}^{\bullet+}$ removes electron density from the carbonyl π bond, weakening it further.

It is also interesting to consider why an $[\text{N}_{\pi}, \text{N}_{\alpha}]$ binding motif is no longer energetically favorable for $\text{His}^{\bullet+}$, as found for $\text{H}^+(\text{His})$. Although an exhaustive search for conformations was not conducted, calculations for $\text{His}^{\bullet+}$ at the present levels of theory find the captodative radical analogue of $[\text{N}_{\pi}, \text{N}_{\alpha}]$ -tggc to lie 42 – 43 kJ/mol higher in energy than the $[\text{N}_{\pi}, \text{CO}]$ ground state. These calculations show that the NH_2 amino group in the $[\text{N}_{\pi}, \text{N}_{\alpha}]$ conformer is no longer nearly planar, becoming pyramidal in order to form the $\text{N}_{\pi}\text{H}\cdots\text{N}_{\alpha}$ hydrogen bond, thereby losing the resonant stabilization of the radical noted above.

3.7. Comparison of experimental IR spectra: $\text{H}^+(\text{His})$ versus $\text{H}^+(\text{HisArg})$ and $\text{H}_2^{2+}(\text{HisArg})$

The Williams group has examined $\text{H}^+(\text{HisArg})$ and $\text{H}_2^{2+}(\text{HisArg})$ with IRMPD spectroscopy and theory [53]. The IRMPD action spectra of $\text{H}^+(\text{His})$ and $\text{H}^+(\text{HisArg})$, the latter protonated on the Arg side chain, have some similar features. The observed carbonyl stretch (1788 cm^{-1}), NH bends ($\sim 1650\text{ cm}^{-1}$), and in-plane hydroxyl bend (1150 cm^{-1}) in the $\text{H}^+(\text{HisArg})$ spectrum are also seen for $\text{H}^+(\text{His})$ at 1778 , 1609 , 1132 cm^{-1} , respectively. A sharp, intense peak at 1080 cm^{-1} is observed for $\text{H}^+(\text{HisArg})$ that is attributed to the neutral histidine side chain on the basis of a comparison to the IR spectra of condensed phase imidazole. Consistent with this assignment is the observation that protonation of the imidazole side chain in the IRMPD spectrum of $\text{H}_2^{2+}(\text{HisArg})$ decreases the intensity of this peak appreciably, becoming a shoulder on the intense 1150 cm^{-1} band. This is comparable to the shoulder observed at 1079 cm^{-1} in the $\text{H}^+(\text{His})$ spectrum, Figure 3, consistent with protonation of the imidazole ring.

3.8. Comparison of experimental IR spectra: $\text{H}^+(\text{His})$ versus $\text{M}^+(\text{His})$

We can also compare the experimental IRMPD spectrum for $\text{H}^+(\text{His})$ with that for alkali metal cation complexes, $\text{M}^+(\text{His})$, where $\text{M}^+ = \text{Li}^+, \text{Na}^+, \text{K}^+, \text{Rb}^+, \text{and } \text{Cs}^+$ [25]. There are several similarities although most bands are broader in the protonated species. The highest frequency

band corresponding to the carbonyl stretch at 1778 cm^{-1} for $\text{H}^+(\text{His})$ is compared to $1732 - 1753\text{ cm}^{-1}$ for the alkali metal complexes. Clearly, the hydrogen bond between the protonated imidazole side-chain nitrogen and backbone amino nitrogen perturbs the carbonyl stretch less than direct binding to the heavier alkali cations. An intense band at $1125 - 1157\text{ cm}^{-1}$ is observed in all spectra, consistent with the fact that the COH bending and C-OH stretching motions of the $\text{H}^+(\text{His})$ $[\text{N}_\pi, \text{N}_\alpha]$ and $\text{M}^+(\text{His})$ $[\text{CO}, \text{N}_\alpha, \text{N}_\pi]$ conformers are similar. The latter complex is a tridentate structure in which the metal cation binds to the carbonyl and amino group of the backbone along with the N_π nitrogen of the side-chain. The shoulder at 1079 cm^{-1} in the $\text{H}^+(\text{His})$ spectrum becomes a sharp, isolated band in the spectra of all $\text{M}^+(\text{His})$ complexes. This is consistent with its identification as a signature peak associated with a neutral imidazole side chain at 1080 cm^{-1} [53,54] and attributed to CN stretches and in-plane CH and NH bends of the side chain ring. Observed bands at $\sim 1580\text{ cm}^{-1}$ in the $\text{K}^+(\text{His}) - \text{Cs}^+(\text{His})$ spectra correspond to an NH_2 bend in the $[\text{CO}, \text{N}_\alpha, \text{N}_\pi]$ spectra. The comparable band in the $\text{H}^+(\text{His})$ spectrum is found at 1609 cm^{-1} , again consistent with more perturbation induced by direct metal binding to the N_α site.

The theoretical results for $\text{K}^+(\text{His}) - \text{Cs}^+(\text{His})$ indicate that the bidentate $[\text{CO}, \text{N}_\pi]$ conformer, in which the metal cation binds to the backbone carbonyl oxygen and nitrogen atom of the imidazole side chain, has an intense band near 1400 cm^{-1} , corresponding to the COH bending motion. This motion is largely unaffected by the increasing cation size, being observed at ~ 1390 , ~ 1385 , and $\sim 1394\text{ cm}^{-1}$ for $\text{K}^+(\text{His}) - \text{Cs}^+(\text{His})$. This is also true for $\text{H}^+(\text{His})$ $[\text{N}_\pi, \text{CO}]$, being predicted at 1387 cm^{-1} and observed at 1399 cm^{-1} . Similarly, weak bands at 742 , 822 , and 1433 cm^{-1} are observed in all cationized spectra, from $\text{Li}^+(\text{His})$ to $\text{Cs}^+(\text{His})$, which seems reasonable as these frequencies correspond to motions that mainly involve groups not directly attached to the ion. Interestingly, the former two frequencies become more prominent as the cation size increases, which is consistent with the increasing populations of $[\text{CO}, \text{N}_\pi]$ and $[\text{COOH}]$ conformations for which these modes gain intensity compared to $[\text{CO}, \text{N}_\alpha, \text{N}_\pi]$. The weak band observed at $\sim 990\text{ cm}^{-1}$ in $\text{H}^+(\text{His})$, largely the NH_2 wag, can be found in all the

$M^+(\text{His})$ spectra but has appreciable intensity only in the $\text{Li}^+(\text{His})$ spectrum, suggesting that the higher charge density may enhance the intensity of this mode. The band observed at 676 cm^{-1} in $\text{H}^+(\text{His})$ is absent in all the $M^+(\text{His})$ spectra, consistent with the predicted IR intensities for these motions, which are greatly reduced for the metal systems.

4. Conclusions

The gas-phase structures of protonated histidine (His) and the side-chain model, protonated 4-phenyl imidazole (PhIm), are examined by infrared multiple photon dissociation (IRMPD) action spectroscopy utilizing light generated by the free electron laser FELIX. Comparison of the measured IRMPD spectra to single photon absorption results calculated at a B3LYP/6-311+G(d,p) level of theory show that $\text{H}^+(\text{His})$ is characterized by a $[\text{N}_\pi, \text{N}_\alpha]$ conformer along with some $[\text{N}_\pi, \text{CO}]$. These conformers have the protonated nitrogen atom of imidazole adjacent to the side-chain (N_π) hydrogen bonding to the backbone amino nitrogen (N_α) and to the backbone carbonyl oxygen, respectively. Comparison of the spectra for $\text{H}^+(\text{PhIm})$ and $\text{H}^+(\text{His})$ allows identification of the vibrational contributions from the protonated imidazole side-chain. Likewise, the IRMPD action spectra of $\text{H}^+(\text{His})$ and $\text{H}^+(\text{histamine})$ [22], which is His without the carboxylic acid on the α -carbon, are found to share many similar features. Comparison of the IRMPD spectra of $\text{H}^+(\text{His})$ with that of the $\text{His}^{\bullet+}$ radical cation provides further evidence for the resonant electron delocalization from the C_α radical center of $\text{His}^{\bullet+}$ that is characteristic of the captodative radical ion identified by Steill et al. [23]. When compared to results for $\text{H}^+(\text{HisArg})$, $\text{H}_2^{2+}(\text{HisArg})$ [53], and $M^+(\text{His})$ [25], the IRMPD action spectrum of $\text{H}^+(\text{His})$ is consistent with protonation of the imidazole ring in only $\text{H}^+(\text{His})$ and $\text{H}_2^{2+}(\text{HisArg})$. Trends in the frequencies observed for $M^+(\text{His})$, where $M^+ = \text{H}^+, \text{Li}^+, \text{Na}^+, \text{K}^+, \text{Rb}^+, \text{and } \text{Cs}^+$, are also explained.

Acknowledgment

Financial support was provided by the National Science Foundation, Grants PIRE-0730072 and CHE-1049580. This work is also part of the research program of FOM, which is

financially supported by the Nederlandse Organisatie voor Wetenschappelijk Onderzoek (NWO). The skillful assistance of the FELIX staff, in particular Lex van der Meer, Britta Redlich, Giel Berden, and Josipa Grzetic, is gratefully acknowledged. In addition, we thank the Center for High Performance Computing at the University of Utah for the generous allocation of computer time.

References

- [1] A. Roth, R.R. Breaker, *Proc. Natl. Acad. Sci. USA* 95 (1998) 6027.
- [2] A.-M.A. Hays, I.R. Vassiliev, J.H. Golbeck, R.J. Debus, *Biochem.* 37 (1998) 11352.
- [3] A. Warshel, S. Russell, *J. Am. Chem. Soc.* 108 (1986) 6569.
- [4] C. Tu, D.N. Silverman, C. Forsman, B.H. Jonsson, S. Lindskog, *Biochem.* 28 (1989) 7913.
- [5] P.A. Frey, S.A. Whitt, J.B. Tobin, *Science* 264 (1994) 1927.
- [6] M.A. Walters, T.G. Spiro, *Inorg. Chem.* 22 (1983) 4014.
- [7] D.S. Caswell, T.G. Spiro, *J. Am. Chem. Soc.* 108 (1986) 6470.
- [8] J. Ramsden, T.G. Spiro, *Biochem.* 28 (1989) 3125.
- [9] E.A. Dierks, S. Hu, K.M. Vogel, A.E. Yu, T.G. Spiro, J.N. Burstyn, *J. Am. Chem. Soc.* 119 (1997) 7316.
- [10] X. Zhao, D. Wang, T.G. Spiro, *Inorg. Chem.* 37 (1998) 5414.
- [11] X. Zhao, D. Wang, T.G. Spiro, *J. Am. Chem. Soc.* 120 (1998) 8517.
- [12] M. Vargek, X. Zhao, Z. Lai, G.L. McLendon, T.G. Spiro, *Inorg. Chem.* 38 (1999) 1372.
- [13] D. Wang, X. Zhao, M. Vargek, T.G. Spiro, *J. Am. Chem. Soc.* 122 (2000) 2193.
- [14] Q. Wu, G. Balakrishnan, A. Pevsner, T.G. Spiro, *J. Phys. Chem. A* 107 (2003) 8047.
- [15] S. Hashimoto, S. Ohsaka, H. Takeuchi, I. Harada, *J. Am. Chem. Soc.* 111 (1989) 8926.
- [16] S. Hashimoto, H. Takeuchi, *J. Am. Chem. Soc.* 120 (1998) 11012.
- [17] S. Hashimoto, H. Takeuchi, *Biochem.* 45 (2006) 9660.
- [18] A. Okada, T. Miura, H. Takeuchi, *Biochem.* 40 (2001) 6053.
- [19] T. Noguchi, Y. Inoue, X.-S. Tang, *Biochem.* 38 (1998) 399.
- [20] Z. Huang, Z. Lin, C. Song, *J. Phys. Chem. A* 111 (2007) 4340.
- [21] K. Hasegawa, T.-A. Ono, T. Noguchi, *J. Phys. Chem. B* 104 (2000) 4253.
- [22] A. Lagutschenkov, J. Langer, G. Berden, J. Oomens, O. Dopfer, *Phys. Chem. Chem. Phys.* 13 (2011) 15644.
- [23] J. Steill, J. Zhao, C.-K. Siu, Y. Ke, U.H. Verkerk, J. Oomens, R.C. Dunbar, A.C. Hopkinson, K.W.M. Siu, *Angew. Chem. Int. Ed.* 47 (2008) 9666.
- [24] J.T. O'Brien, J.S. Prell, G. Berden, J. Oomens, E.R. Williams, *Int. J. Mass Spectrom.* 297 (2010) 116.
- [25] M. Citir, C.S. Hinton, J. Oomens, J.D. Steill, P.B. Armentrout, *J. Phys. Chem. A* 116 (2012) 1532.
- [26] D. Oepts, A.F.G. van der Meer, P.W. van Amersfoort, *Infrared Phys. Technol.* 36 (1995) 297.
- [27] J.J. Valle, J.R. Eyler, J. Oomens, D.T. Moore, A.F.G.v.d. Meer, G.v. Heldon, G. Meijer, C.L. Hendrickson, A.G. Marschall, G.T. Blakney, *Rev. Sci. Instrum.* 76 (2005) 023103.

- [28] N.C. Polfer, J. Oomens, D.T. Moore, G. von Helden, G. Meijer, R.C. Dunbar, J. Am. Chem. Soc. 128 (2006) 517.
- [29] N.C. Polfer, J. Oomens, Phys. Chem. Chem. Phys. 9 (2007) 3804.
- [30] R.M. Moision, P.B. Armentrout, J. Phys. Chem. A 106 (2002) 10350.
- [31] D.A. Pearlman, D.A. Case, J.W. Caldwell, W.R. Ross, T.E. Cheatham, S. DeBolt, D. Ferguson, G. Seibel, P. Kollman, Comp. Phys. Commun. 91 (1995) 1.
- [32] E.J. Bylaska, W.A. deJong, K. Kowalski, T.P. Straatsma, M. Valiev, D. Wang, E. Aprà, T.L. Windus, S. Hirata, M.T. Hackler, Y. Zhao, P.-D. Fan, R.J. Harrison, M. Dupuis, D.M.A. Smith, J. Nieplocha, V. Tipparaju, M. Krishnan, A.A. Auer, M. Nooijen, E. Brown, G. Cisneros, G.I. Fann, H. Früchtl, J. Garza, K. Hirao, R. Kendall, J.A. Nichols, K. Tsemekhman, K. Wolinski, J. Anchell, D. Bernholdt, P. Borowski, T. Clark, D. Clerc, H. Dachsel, M. Deegan, K. Dyall, D. Elwood, E. Glendening, M. Gutowski, A. Hess, J. Jaffe, B. Johnson, J. Ju, R. Kobayashi, R. Kutteh, Z. Lin, R. Littlefield, X. Long, B. Meng, T. Nakajima, S. Niu, L. Pollack, M. Rosing, G. Sandrone, M. Stave, H. Taylor, G. Thomas, J.v. Lenthe, A. Wong, Z. Zhang, NWChem, A Computational Chemistry Package for Parallel Computers. Pacific Northwest National Laboratory, Richland, Washington 99352, 2003.
- [33] C.C. Roothaan, Rev. Mod. Phys. 23 (1951) 69.
- [34] J.S. Binkley, J.A. Pople, W.J. Hehre, J. Am. Chem. Soc. 102 (1980) 939.
- [35] M.J. Frisch, G.W. Trucks, H.B. Schlegel, G.E. Scuseria, M.A. Robb, J.R. Cheeseman, G. Scalmani, V. Barone, B. Mennucci, G.A. Petersson, H. Nakatsuji, M. Caricato, X. Li, H.P. Hratchian, A.F. Izmaylov, J. Bloino, G. Zheng, J.L. Sonnenberg, M. Hada, M. Ehara, K. Toyota, R. Fukuda, J. Hasegawa, M. Ishida, T. Nakajima, Y. Honda, O. Kitao, H. Nakai, T. Vreven, J. Montgomery, J. A. , J.E. Peralta, F. Ogliaro, M. Bearpark, J.J. Heyd, E. Brothers, K.N. Kudin, V.N. Staroverov, R. Kobayashi, J. Normand, K. Raghavachari, A. Rendell, J.C. Burant, J.M. Millam, S.S. Iyengar, J. Tomasi, M. Cossi, N. Rega, J.M. Millam, M. Klene, J.E. Knox, J.B. Cross, V. Bakken, C. Adamo, J. Jaramillo, R. Gomperts, R.E. Stratmann, O. Yazyev, A.J. Austin, R. Cammi, C. Pomelli, J.W. Ochterski, R.L. Martin, K. Morokuma, V.G. Zakrzewski, G.A. Voth, P. Salvador, J.J. Dannenberg, S. Dapprich, A.D. Daniels, O. Farkas, J.B. Foresman, J.V. Ortiz, J. Cioslowski, D.J. Fox, Gaussian 09, Revision A.02. Gaussian Inc., Pittsburgh, PA, 2009.
- [36] A.D. Becke, J. Chem. Phys. 98 (1993) 5648.
- [37] R. Ditchfield, W.J. Hehre, J.A. Pople, J. Chem. Phys. 54 (1971) 724.
- [38] A.D. McLean, G.S. Chandler, J. Chem. Phys. 72 (1980) 5639.
- [39] J.B. Foresman, A.E. Frisch, Exploring Chemistry with Electronic Structure Methods, Gaussian, Inc., Pittsburgh, PA, 1996.
- [40] N.C. Polfer, J. Oomens, R.C. Dunbar, Phys. Chem. Chem. Phys. 8 (2006) 2744.
- [41] M.F. Bush, J. Oomens, R.J. Saykally, E.R. Williams, J. Phys. Chem. A 112 (2008) 8578.
- [42] M.F. Bush, J. Oomens, R.J. Saykally, E.R. Williams, J. Am. Chem. Soc. 130 (2008) 6463.
- [43] A.L. Heaton, V.N. Bowman, J. Oomens, J.D. Steill, P.B. Armentrout, J. Phys. Chem. A 113 (2009) 5519.
- [44] D.R. Carl, T.E. Cooper, J. Oomens, J.D. Steill, P.B. Armentrout, Phys. Chem. Chem. Phys. 12 (2010) 3384.
- [45] M. Citir, E.M.S. Stennett, J. Oomens, J.D. Steill, M.T. Rodgers, P.B. Armentrout, Int. J. Mass Spectrom. 297 (2010) 9.
- [46] S.J. Ye, P.B. Armentrout, J. Phys. Chem. A 112 (2008) 3587.

- [47] T.E. Cooper, D.R. Carl, P.B. Armentrout, J. Phys. Chem. A 113 (2009) 13727.
- [48] P.B. Armentrout, A.L. Heaton, S.J. Ye, J. Phys. Chem. A 115 (2011) 11144.
- [49] D.R. Carl, P.B. Armentrout, J. Phys. Chem. A 116 (2012) 3802.
- [50] H.E. Aribi, G. Orlova, A.C. Hopkinson, K.W.M. Siu, J. Phys. Chem. A 108 (2004) 3844.
- [51] F. Rogalewicz, Y. Hoppilliard, G. Ohanessian, Int. J. Mass Spectrom. 195/196 (2000) 565.
- [52] IUPAC. Compendium of Chemical Terminology, 2nd ed. (the "Gold Book"). Compiled by A. D. McNaught and A. Wilkinson. Blackwell Scientific Publications, Oxford (1997). XML on-line corrected version: <http://goldbook.iupac.org> (2006-) created by M. Nic, J. Jirat, B. Kosata; updates compiled by A. Jenkins. ISBN 0-9678550-9-8. doi:10.1351/goldbook.
- [53] J.S. Prell, J.T. O'Brien, J.D. Steill, J. Oomens, E.R. Williams, J. Am. Chem. Soc. 131 (2009) 11442.
- [54] M.C. Sister, J.L. Walter, Spectrochim. Acta, Part A 24 (1968) 237.

TABLE 1: 298 K Free Energies (0 K Relative Enthalpies) in kJ/mol of Low-Lying Conformers of $H^+(\text{His})^a$

Structure	Dihedral	B3LYP	B3P86	MP2(full)
$[N_\pi, N_\alpha]$	tggc	0.0 (0.0)	0.0 (0.4)	0.0 (0.0)
	tgtc	0.6 (0.8)	1.1 (1.7)	5.1 (5.3)
	tttc	4.2 (5.5)	4.9 (6.7)	8.7 (10.1)
	ttgc	4.4 (3.9)	5.1 (5.1)	4.1 (3.7)
	cggc	31.0 (30.8)	31.4 (31.6)	29.7 (29.5)
	cgtc	34.8 (35.1)	35.2 (35.9)	39.7 (40.0)
TS ($[N_\pi, N_\alpha] \rightarrow [N_\alpha, N_\pi]$)	tggc	8.2 (6.0)	1.7 (0.0)	4.9 (2.8)
	tgtc	7.2 (5.6)	1.5 (0.3)	7.6 (6.0)
	tttc	15.5 (15.3)	10.1 (10.3)	14.9 (14.7)
	ttgc	17.2 (15.3)	11.4 (9.9)	12.7 (10.8)
	cggc	41.7 (40.0)	35.0 (33.7)	38.2 (36.5)
	cgtc	41.3 (39.6)	35.2 (33.9)	42.3 (40.6)
$[N_\alpha, N_\pi]$	tggc	8.5 (7.2)	5.1 (4.3)	2.7 (1.4)
	tgtc	6.6 (6.0)	4.1 (3.9)	3.7 (3.1)
	tttc	17.7 (18.4)	15.8 (16.9)	14.1 (14.8)
	ttgc	20.0 (19.0)	17.4 (16.9)	12.8 (11.9)
	cggc	42.4 (41.4)	38.6 (38.0)	37.3 (36.3)
	cgtc	40.1 (39.3)	37.2 (36.8)	37.9 (37.0)
$[N_\pi, \text{CO}]$	ctg ₊ g ₋	3.9 (1.8)	1.7 (0.0)	12.9 (10.8)
	ttg ₋ g ₊ (g)	4.8 (5.0)	7.3 (7.9)	8.1 (8.3)
	ttg ₋ g ₊ (t)	4.9 (4.8)	7.2 (7.4)	11.2 (11.0)
	ttg ₊ g ₋ (t)	5.2 (5.9)	6.8 (7.8)	13.9 (14.5)
	ttg ₊ g ₋ (g)	8.6 (8.0)	10.5 (10.3)	16.1 (15.4)
	ctg ₋ g ₊	17.7 (15.8)	16.9 (15.4)	23.5 (21.5)
	ctg ₋ g ₊ (t)	28.7 (29.6)	30.8 (32.1)	35.1 (36.0)
	cggg	30.0 (30.8)	31.6 (32.8)	34.1 (34.9)

[N _π ,OH]	tcg_g+(g)	23.1 (26.4)	26.3 (30.0)	23.2 (26.4)
	tg_g+g-(t)	29.2 (30.2)	33.1 (34.4)	34.9 (35.8)
	tg_g+g-(g)	31.5 (32.3)	35.0 (36.2)	36.7 (37.5)
	tg+g_g+(t)	33.5 (35.9)	38.1 (41.0)	36.2 (38.7)

^a All values calculated at the level of theory indicated using the 6-311+G(2d,2p) basis set with structures and zero-point energies calculated at the B3LYP/6-311+G(d,p) level of theory.

Ground state species are identified in bold. Italics indicates species that collapse because the TS energy is lower.

Table 2: Experimental vibrational frequencies (cm^{-1}) of $\text{H}^+(\text{His})$ compared to B3LYP/6-311+G(d,p) frequencies of the $[\text{N}_\pi, \text{N}_\alpha]$ -tggc and $[\text{N}_\pi, \text{CO}]$ -ctg₊g₋ conformers.

$\text{H}^+(\text{His})$ $\nu_{\text{exp}}^{\text{a}}$	$\text{H}^+(\text{His}), \nu_{\text{cal}}^{\text{b}}$ $[\text{N}_\pi, \text{N}_\alpha]$ -tggc	$\text{H}^+(\text{His}), \nu_{\text{cal}}^{\text{b}}$ $[\text{N}_\pi, \text{CO}]$ -ctg ₊ g ₋	Vibration ^c
1778	1775 (266)	—	σ_{CO}
1747	—	1736 (291)	$\sigma_{\text{CO}} / \beta_{\text{NH}} (\text{N}_\pi)$
1609	1610 (76)	1608 (129)	$\sigma_{\text{CC}} (\text{C}_4\text{C}_5) / \beta_{\text{NH}} (\text{N}_\pi, \text{N}_\tau) / \beta_{\text{CH}} (\text{C}_5) = \nu_5(\text{Im})$
	1593 (79)	1623 (44)	β_{NH_2} (scissor)
	1512 (12)	1516 (8)	$\sigma_{\text{CN}} (\text{C}_2) / \beta_{\text{CH}} (\text{C}_2, \text{C}_5) = \nu_6(\text{Im})$
1433	1461 (15)	1459 (14)	$\beta_{\text{NH}} (\text{N}_\tau) / \sigma_{\text{CN}} (\text{N}_\tau)$
	1444 (18)	1446 (16)	β_{CH_2} (scissor, C_β)
	—	1408 (19)	$\beta_{\text{NH}} (\text{N}_\pi) / \sigma_{\text{CN}} (\text{C}_4\text{N}_\pi) / \beta_{\text{COH}}$
1399	1392 (54)	—	$\beta_{\text{NH}} (\text{N}_\pi) / \sigma_{\text{CN}} (\text{N}_\pi) = \nu_7(\text{Im})$
	1391 (26)	—	$\beta_{\text{CH}} (\text{C}_\alpha) / \beta_{\text{CH}_2}$ (wag) / τ_{NH_2}
	—	1387 (568)	β_{COH}
	—	1367 (7)	$\beta_{\text{CH}} (\text{C}_\alpha) / \beta_{\text{NH}_2}$ (twist)
1340	1341 (1)	1329 (3)	β_{CH_2} (wag) / $\beta_{\text{CH}} (\text{C}_\alpha)$
1306	1299 (31)	1309, 1267 (7,48)	$\beta_{\text{CH}} (\text{C}_\alpha) / \beta_{\text{CH}} (\text{C}_\beta) / \beta(\text{Im})$
	1292 (21)	1217 (2)	$\beta_{\text{COH}} / \beta_{\text{CH}} (\text{C}_\alpha)$
	1252 (4)	—	$\sigma_{\text{CCN}} (\text{C}_4) / \beta_{\text{CH}} (\text{C}_\alpha) / \beta_{\text{NH}_2}$ (twist) / β_{CH_2} (twist)
	1239 (6)	1249 (20)	$\sigma_{\text{CN}} (\text{C}_5\text{N}_\tau) / \beta_{\text{CH}} (\text{C}_5) / \beta_{\text{CH}_2}$ (wag) = $\nu_{10}(\text{Im})$
	1205 (2)	1185 (3)	β_{CH_2} (twist) / $\beta_{\text{CH}} (\text{C}_\alpha) = \nu_8(\text{Im})$
	1188 (17)	1150 (2)	β_{NH_2} (twist) / $\beta_{\text{CH}} (\text{C}_\alpha) / \beta_{\text{CH}} (\text{C}_\beta)$
	1164 (8)	1165 (4)	$\beta_{\text{CH}} (\text{C}_2) / \beta_{\text{NH}} (\text{N}_\tau) = \nu_9(\text{Im})$
1132	1139 (175)	—	$\beta_{\text{COH}} / \sigma_{\text{CO(H)}}$
	1107 (130)	1126 (172)	$\beta_{\text{NH}} (\text{N}_\pi) / \beta_{\text{NH}} (\text{N}_\tau) / \sigma_{\text{CN}} (\text{C}_2) / \beta_{\text{CH}} (\text{C}_5) = \nu_{12}(\text{Im})$
1079	—	1079 (20)	$\sigma_{\text{CN}} (\text{N}_\alpha)$
	—	1067 (17)	$\sigma_{\text{CN}} (\text{C}_5\text{N}_\tau) / \beta_{\text{CH}} (\text{C}_5) / \beta_{\text{NH}} (\text{N}_\tau)$
	1066 (4)	—	$\sigma_{\text{CN}} (\text{C}_5\text{N}_\tau) / \beta_{\text{CH}} (\text{C}_5)$ and $\sigma_{\text{CN}} (\text{N}_\alpha) = \nu_{11}(\text{Im})$
	1061 (40)	—	$\sigma_{\text{CN}} (\text{C}_5\text{N}_\tau) / \beta_{\text{CH}} (\text{C}_5)$ and $\sigma_{\text{CN}} (\text{N}_\alpha) = \nu_{11}(\text{Im})$

990	—	1009 (38)	$\sigma_{CC} (C_{\alpha}C_{\beta}) / \beta_{NH_2} (\text{twist})$
	1002 (107)	—	$\sigma_{CN} (N_{\pi}, \text{sym}) / \gamma_{NH} (N_{\pi}) / \beta_{NH_2} (\text{wag}) = \nu_{14}(\text{Im})$
	—	987 (30)	$\gamma_{NH} (N_{\pi}) = \nu_{21}(\text{Im})$
	973 (55)	—	$\beta_{NH_2} (\text{wag}) / \sigma_{CN} (CN_{\alpha})$
923	955 (53)	960 (80)	$\gamma_{NH} (N_{\pi}) / \beta_{CH} (C_2) = \nu_{21}(\text{Im})$
	946 (41)	933 (18)	$\tau_{NH_2} / \beta_{CH_2} / \gamma_{NH} (N_{\pi})$
	925 (14)	924 (9)	$\beta (CN_{\tau}C) = \nu_{15}(\text{Im})$
	889 (3)	—	$\sigma_{CC} (C_{\beta}C_{\alpha})$
	—	882 (83)	γ_{COH}
	829 (6)	—	$\beta_{CC} (C_{\beta}) / \beta_{CH} (C_2, \text{twist}) / \beta_{NH_2} (\text{wag})$
822	823 (39)	830 (33)	$\gamma_{CH} (\text{in phase}, C_2 + C_5) = \nu_{17}(\text{Im})$
	782 (4)	—	$\gamma_{CH} (\text{out of phase}, C_2 + C_5) = \nu_{16}(\text{Im})$
798	—	809 (137)	$\beta_{NH_2} (\text{wag})$
	—	787 (21), 782 (10)	$\sigma_{CC} (C_{\alpha}CO) / \gamma_{CH} (C_2C_5) / \beta_{OCO} / \beta_{NH_2} (\text{wag})$
742	—	738 (17)	$\beta_{OCO} / \sigma_{CC} (C_{\alpha}C_{\beta}) / \gamma_{CH} (C_5)$
	734 (19)	—	$\beta_{CCC} (C_{\beta}) / \beta_{OCO} / \gamma_{CH} (C_5)$
	—	711 (12)	$\beta_{CCC} (C_{\beta}) / \gamma_{OCO}$
676	686 (75)	—	$\gamma_{COH} / \gamma_{CN/CC} = \nu_{18}(\text{Im})$
	669 (54)	670 (63)	$\gamma_{NH} (N_{\tau})$
	—	639 (2)	$\gamma_{CN/CC}$
	634 (39)	—	$\gamma_{COH} / \gamma_{CN/CC} = \nu_{20}(\text{Im})$
609	606 (26)	—	$\gamma_{COH} / \sigma_{CC} (C_4C_{\beta})$
	—	606 (52)	$\gamma_{CNC} (N_{\tau})$
	605 (51)	—	$\gamma_{COH} / \gamma_{CN/CC} = \nu_{19}(\text{Im})$
	—	578 (2)	$\beta_{OCC} / \beta_{CCN} (N_{\alpha})$
	573 (31)	—	$\gamma_{COH} / \beta_{OCO}$

^a Peak positions taken from the IRMPD spectrum in Fig. 3. ^b Vibrational frequencies (cm^{-1}) scaled by 0.975 and IR intensities (km/mol) are given in parentheses. ^c The notation σ , β , and γ refers to stretch, in-plane bend, and out-of-plane bend modes, respectively. $\nu_i(\text{Im})$ denote corresponding normal modes of imidazole taken from ref. [22].

Table 3: Experimental vibrational frequencies (cm^{-1}) of H^+ (4-phenyl imidazole) compared to B3LYP/6-311+G(d,p) frequencies.

$\text{H}^+(\text{PhIm})$ ν_{exp}^a	$\text{H}^+(\text{PhIm}),$ ν_{cal}^b	Vibration ^c
1606	1609 (126)	$\sigma_{\text{CC}}(\text{C}_4\text{C}_5) / \beta_{\text{NH}}(\text{N}_\pi, \text{N}_\tau) / \beta_{\text{CH}}(\text{C}_5) = \nu_5(\text{Im})$
	1596 (2)	$\sigma_{\text{CC}}(\text{Ph}, \text{sym}) / \beta_{\text{CH}}(\text{Ph})$
	1575 (9)	$\sigma_{\text{CC}}(\text{Ph}, \text{antisym}) / \beta_{\text{CH}}(\text{Ph})$
1482	1513 (12)	$\sigma_{\text{CN}}(\text{C}_2) / \beta_{\text{CH}}(\text{C}_2, \text{C}_5) = \nu_6(\text{Im})$
	1493 (5)	$\beta_{\text{CH}}(\text{Ph}) / \sigma_{\text{CC}}(\text{C}_4\text{C}_{\text{Ph}}) / \beta_{\text{NH}}(\text{N}_\tau)$
1448	1456 (25)	$\beta_{\text{NH}}(\text{N}_\tau) / \sigma_{\text{CN}}(\text{N}_\tau)$
	1444 (12)	$\beta_{\text{CH}}(\text{Ph}) / \sigma_{\text{CC}}(\text{Ph}, \text{antisym})$
	1401 (2)	$\beta_{\text{NH}}(\text{N}_\pi) / \sigma_{\text{CN}}(\text{N}_\pi) = \nu_7(\text{Im})$
1339	1326 (3)	$\beta_{\text{CH}}(\text{Ph}, \text{antisym})$
	1302 (1)	$\sigma_{\text{CC}}(\text{Ph}, \text{antisym}) / \beta_{\text{CH}}(\text{Ph})$
~1300 (tail)	1281 (12)	$\sigma_{\text{CN}}(\text{C}_5\text{N}_\tau) / \beta_{\text{CH}}(\text{C}_5) / \beta_{\text{CH}_2}(\text{wag}) = \nu_{10}(\text{Im})$
	1234 (0.2)	$\sigma_{\text{CN}}(\text{C}_4\text{N}_\pi) / \beta_{\text{CH}}(\text{C}_5) / \beta_{\text{NH}}(\text{N}_\pi) = \nu_8(\text{Im})$
	1181 (1)	$\beta_{\text{CH}}(\text{Ph}, \text{sym})$
1152	1171 (12)	$\beta_{\text{CH}}(\text{C}_2) / \beta_{\text{NH}}(\text{N}_\tau) = \nu_9(\text{Im})$
	1164 (0.1)	$\beta_{\text{CH}}(\text{Ph})$
	1149 (18)	$\beta_{\text{CH}}(\text{C}_2) / \beta_{\text{NH}}(\text{N}_\pi) = \nu_{12}(\text{Im})$
	1084 (10)	$\beta_{\text{CH}}(\text{Ph}) / \sigma_{\text{CC}}(\text{Ph})$
1064	1070 (21)	$\sigma_{\text{CN}}(\text{C}_5\text{N}_\tau) / \beta_{\text{CH}}(\text{C}_5) = \nu_{11}(\text{Im})$
	1046 (14)	$\sigma_{\text{CN}}(\text{C}_4\text{N}_\pi) / \beta_{\text{CH}}(\text{C}_5) / \beta_{\text{CH}}(\text{Ph})$
996	990 (4)	$\sigma_{\text{CC}}(\text{Ph}, \text{sym})$
	970 (1)	$\gamma_{\text{CH}}(\text{Ph})$
937	937 (5)	$\sigma_{\text{CN}}(\text{N}_\pi, \text{sym}) = \nu_{14}(\text{Im})$
	918 (1)	$\gamma_{\text{CH}}(\text{Ph})$
	915 (3)	$\beta(\text{NC}_2\text{N}) = \nu_{15}(\text{Im})$
	830 (1)	$\gamma_{\text{CH}}(\text{Ph}, \text{out of phase})$
	821 (1)	$\gamma_{\text{CH}}(\text{in phase}, \text{C}_2 + \text{C}_5) = \nu_{17}(\text{Im})$
	786 (11)	$\gamma_{\text{CH}}(\text{out of phase}, \text{C}_2 + \text{C}_5) = \nu_{16}(\text{Im})$
	752 (81)	$\gamma_{\text{CH}}(\text{Ph})$

~710 (wide)	701 (149)	γ_{NH} (in phase, $N_{\pi} + N_{\tau}$)
	687 (30)	$\gamma_{\text{CH}}(\text{Ph})$
	677 (3)	$\beta_{\text{CC}}(\text{Ph})$
	664 (6)	$\gamma_{\text{CN/CC}} = \nu_{18}(\text{Im})$
	649 (0.2)	γ_{NH} (out of phase, $N_{\pi} + N_{\tau}$)
	603 (48)	$\gamma_{\text{CN/CC}} = \nu_{19}(\text{Im})$

^a Peak positions taken from the IRMPD spectrum in Fig. 4. ^b Vibrational frequencies (cm^{-1}) scaled by 0.975 and IR intensities (km/mol) are given in parentheses. ^c The notation σ , β , γ , and τ refers to stretch, in-plane bend, out-of-plane bend, and torsional modes, respectively. Im and Ph refer to imidazole and phenyl, respectively. $\nu_i(\text{Im})$ denote corresponding normal modes of imidazole taken from ref. [22].

Figure Captions

Fig. 1. Structures of the $H^+(\text{His})$ complexes calculated at the B3LYP/6-311+G(d,p) level of theory. Dashed lines indicate hydrogen bonds shorter than 2.3 Å. Atomic labels of protonated histidine are shown in one panel.

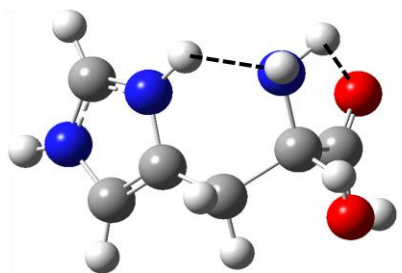
Fig. 2. Relaxed potential energy surfaces of $H^+(\text{His})$ and $H^+(\text{histamine})$ along the $N_\pi\text{-H-N}_\alpha$ coordinate linking the $[N_\pi, N_\alpha]$ (left side) and $[N_\alpha, N_\pi]$ (right side) conformers calculated at the B3LYP/6-311+G(d,p) level. The energy zero is set to the zero point energy of the harmonic frequency in the $[N_\pi, N_\alpha]$ potential well.

Fig. 3. Comparison of the experimental IRMPD action spectrum for $H^+(\text{His})$ with IR spectra for three low-lying conformations predicted at the B3LYP/6-311+G(d,p) level of theory.

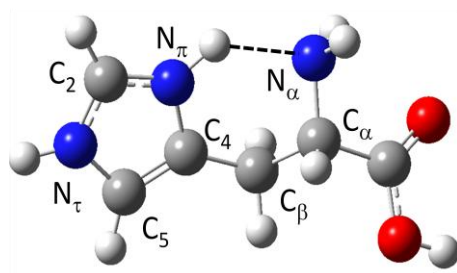
Fig. 4. Comparison of the experimental IRMPD action spectra for $H^+(\text{His})$ and $H^+(\text{PhIm})$ with the IR spectrum for protonated 4-phenyl imidazole predicted at the B3LYP/6-311+G(d,p) level of theory. The last panel also shows the calculated structure.

Fig. 5. Comparison of the experimental IRMPD action spectra for $H^+(\text{His})$ with IR spectra for $H^+(\text{His})[N_\pi, N_\alpha]\text{-tggc}$ and $H^+(\text{histamine})$ predicted at the B3LYP/6-311+G(d,p) level of theory.

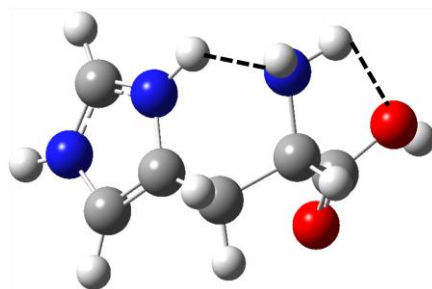
$[N_\pi, N_\alpha]$



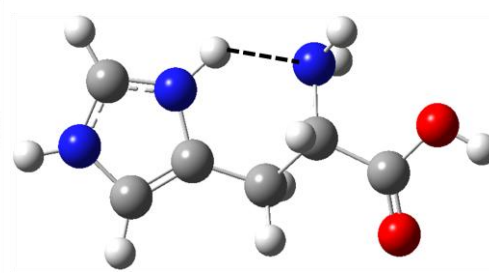
tggc



tgtc

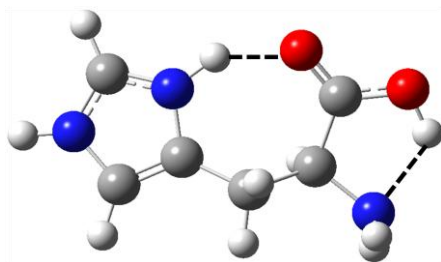


ttgc

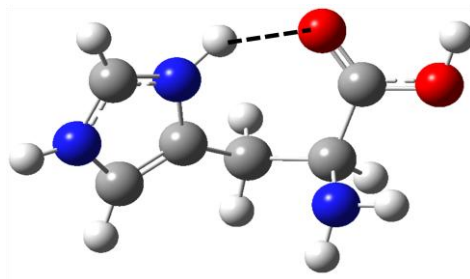


ttcc

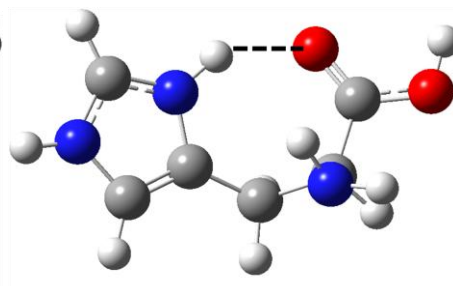
$[N_\pi, CO]$



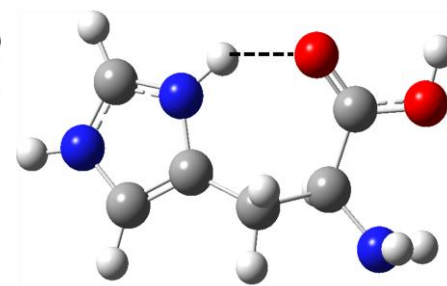
ctg+g₋



ttg₋g₊(g)



ttg₋g₊(t)



ttg₊g₋(t)

Figure 1

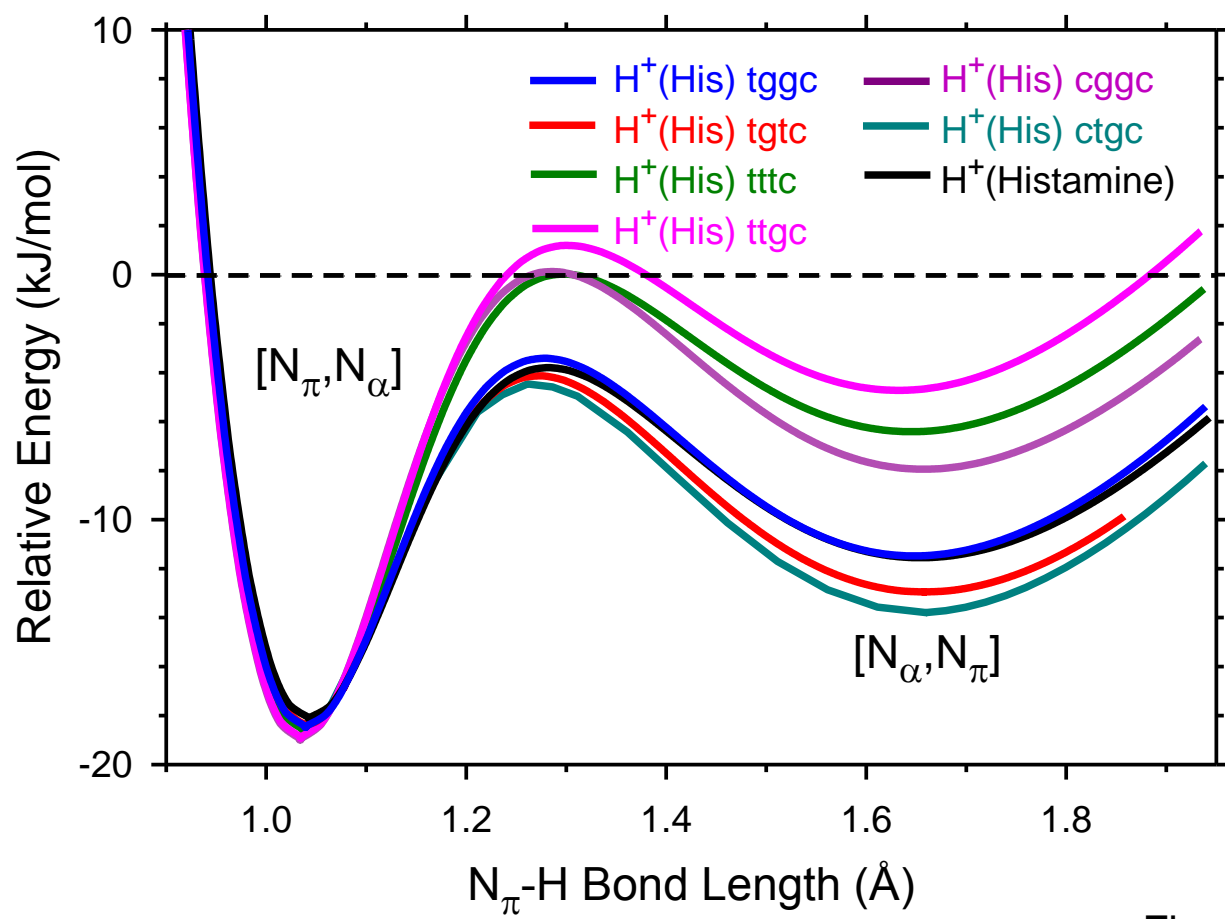


Figure 2

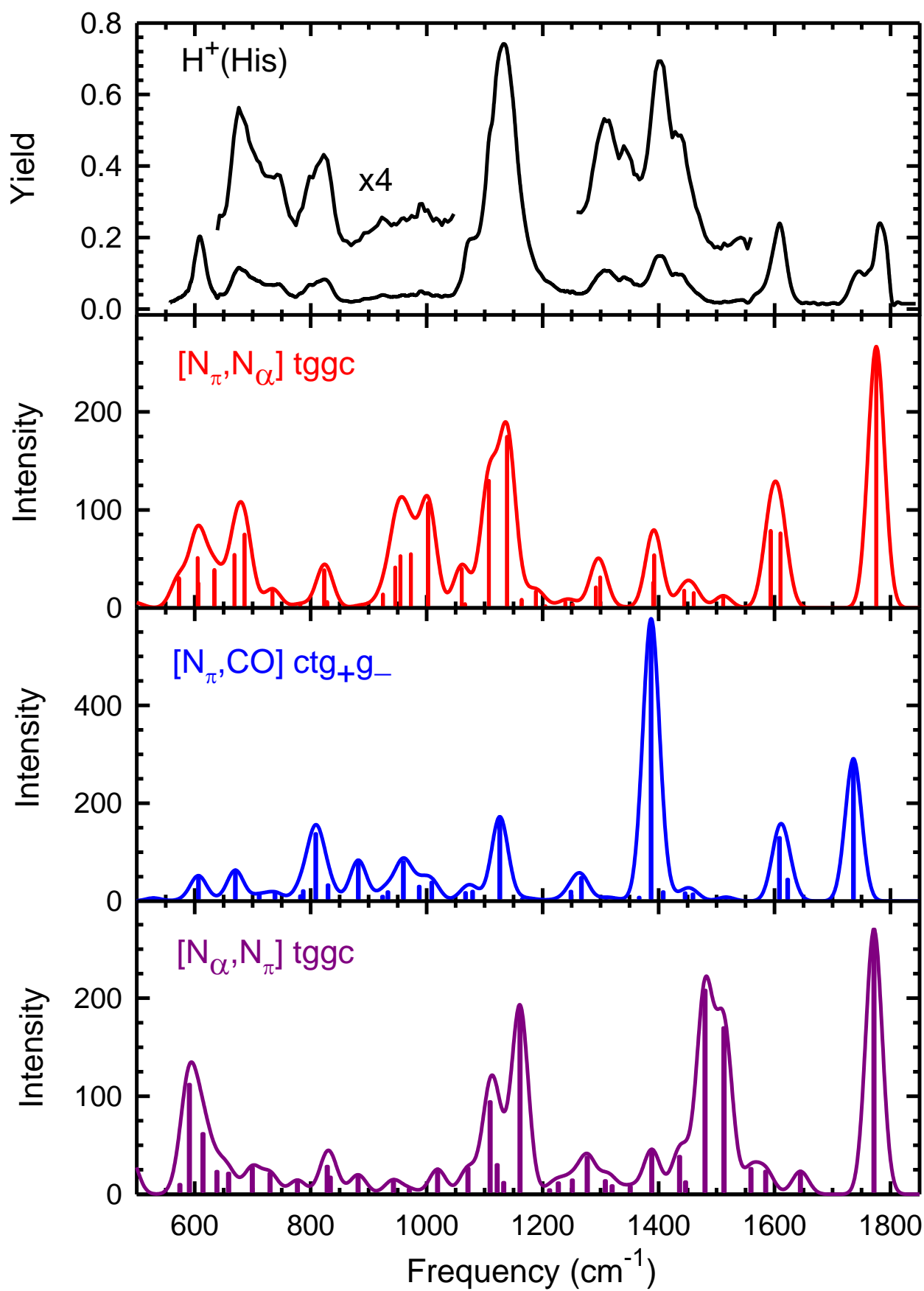


Figure 3

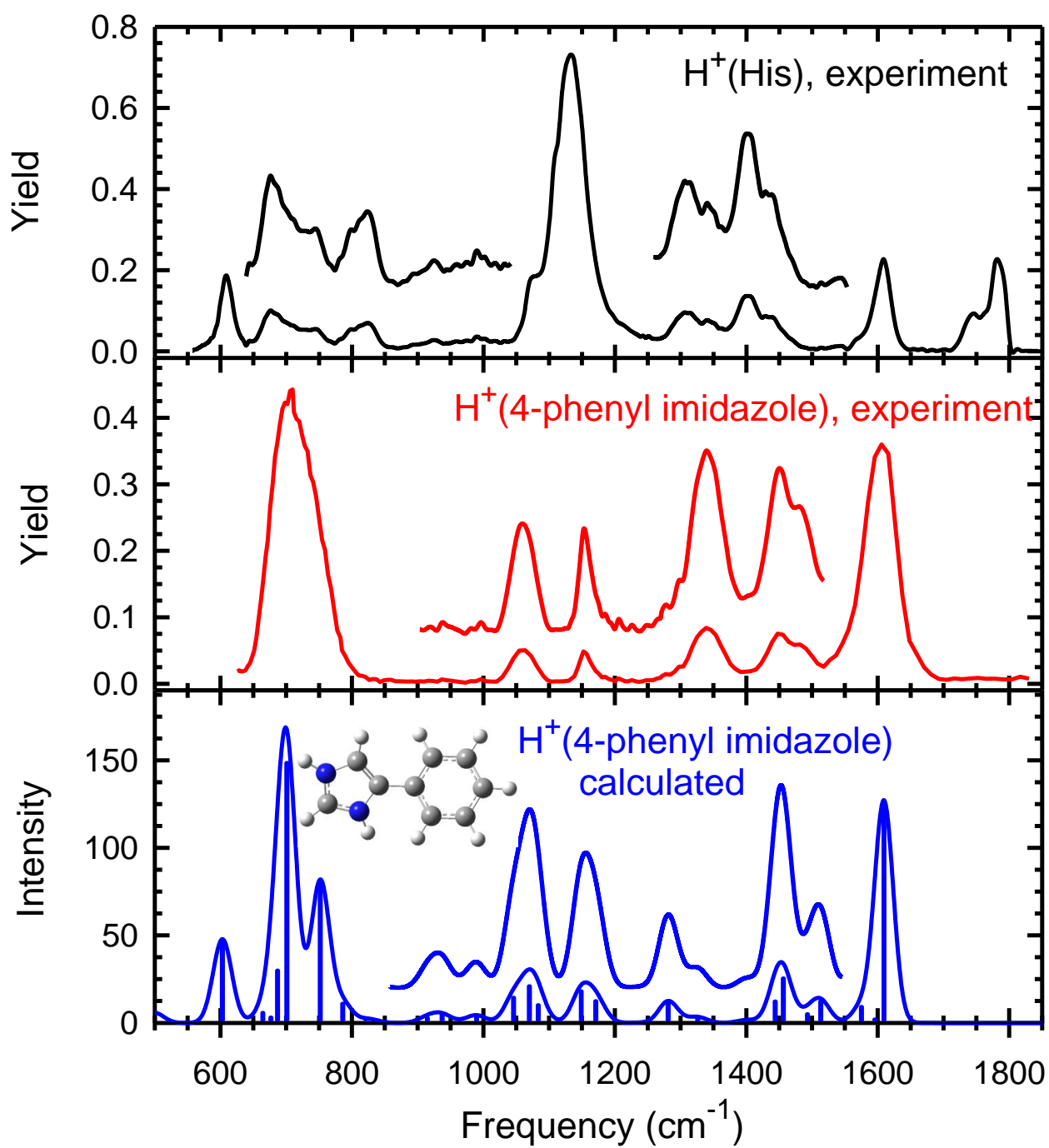


Figure 4

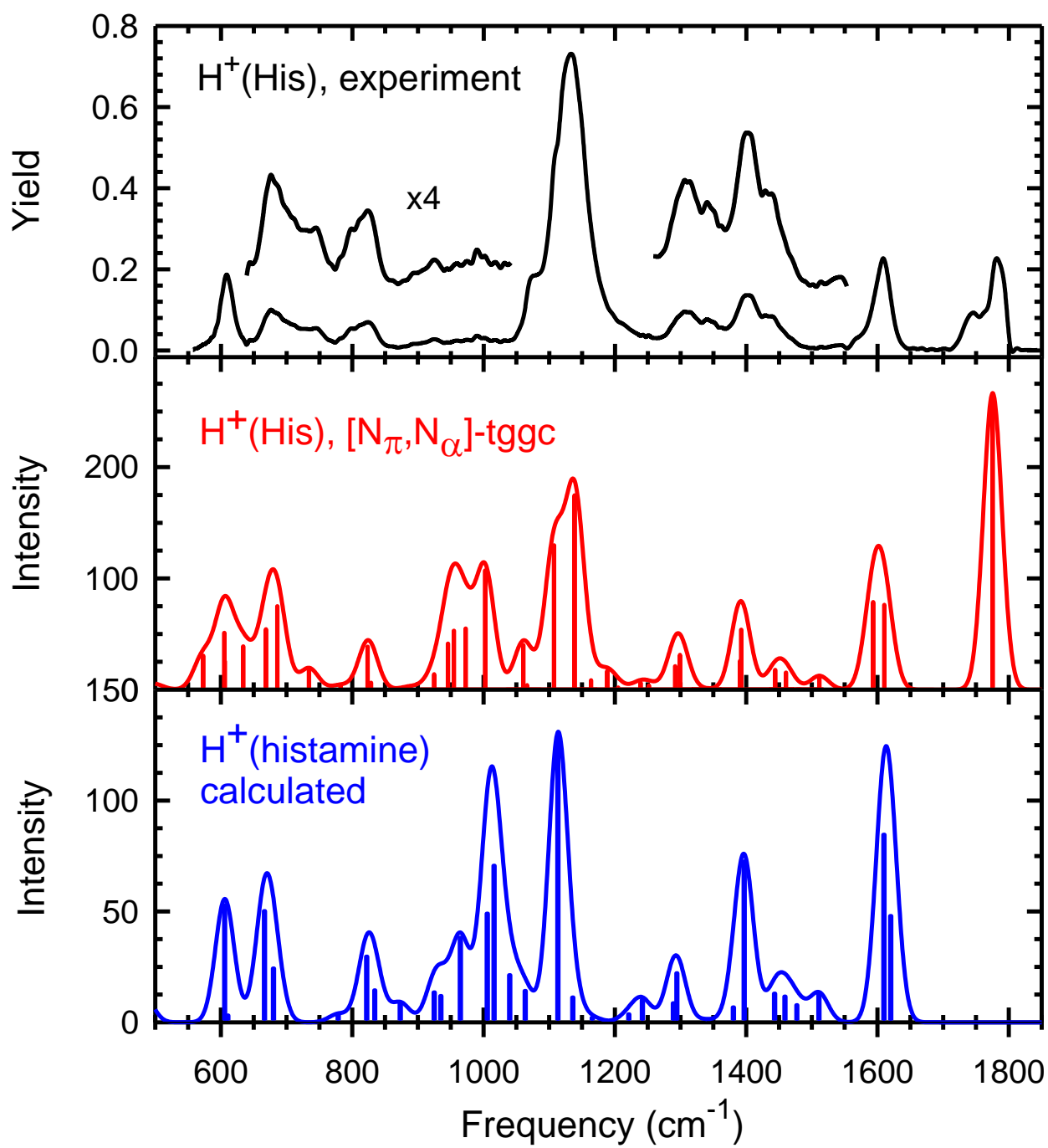


Figure 5

Supporting Information for
Infrared Multiple Photon Dissociation Spectroscopy of Protonated Histidine and 4-Phenyl
Imidazole

by Murat Citir, Christopher S. Hinton, Jos Oomens, Jeffrey D. Steill, and P. B. Armentrout

Figure Captions

Figure S1. Comparison of the experimental $\text{H}^+(\text{His})$ (m/z 156) depletion spectrum (top, purple) and the IRMPD action spectrum for the m/z 110 product ion (loss of $\text{H}_2\text{O} + \text{CO}$) both uncorrected (red) and corrected (blue) for laser power.

Figure S2. Geometries of all conformers of $\text{H}^+(\text{His})$ calculated at the B3LYP/6-311+G(d,p) level of theory. Hydrogen bonding interactions shorter than 2.3 Å are indicated by dashed lines and lengths in Å.

Figure S3. Comparison of predicted IR spectra for all conformers of $\text{H}^+(\text{His})$ calculated at the B3LYP/6-311+G(d,p) level of theory.

Figure S4. Comparison of predicted harmonic and anharmonic (unscaled) IR spectra for $\text{H}^+(\text{His})$ $[\text{N}_\pi, \text{N}_\alpha]$ -tggc and $[\text{N}_\pi, \text{CO}]$ -ctg+g₋ at the B3LYP/6-311+G(d,p) level of theory.

Figure S5. Comparison of predicted IR spectra for four representative low energy conformations of His at the B3LYP/6-311+G(d,p) level of theory. 298 K Gibbs free energies (kJ/mol) are in parenthesis. All values calculated at the B3LYP/6-311+G(2d,2p), B3P86/6-311+G(2d,2p), and MP2(full)/6-311+G(2d,2p) level of theory with structures and zero point energies calculated at the B3LYP/6-311+G(d,p) level of theory. Dashed lines indicate hydrogen bonds.

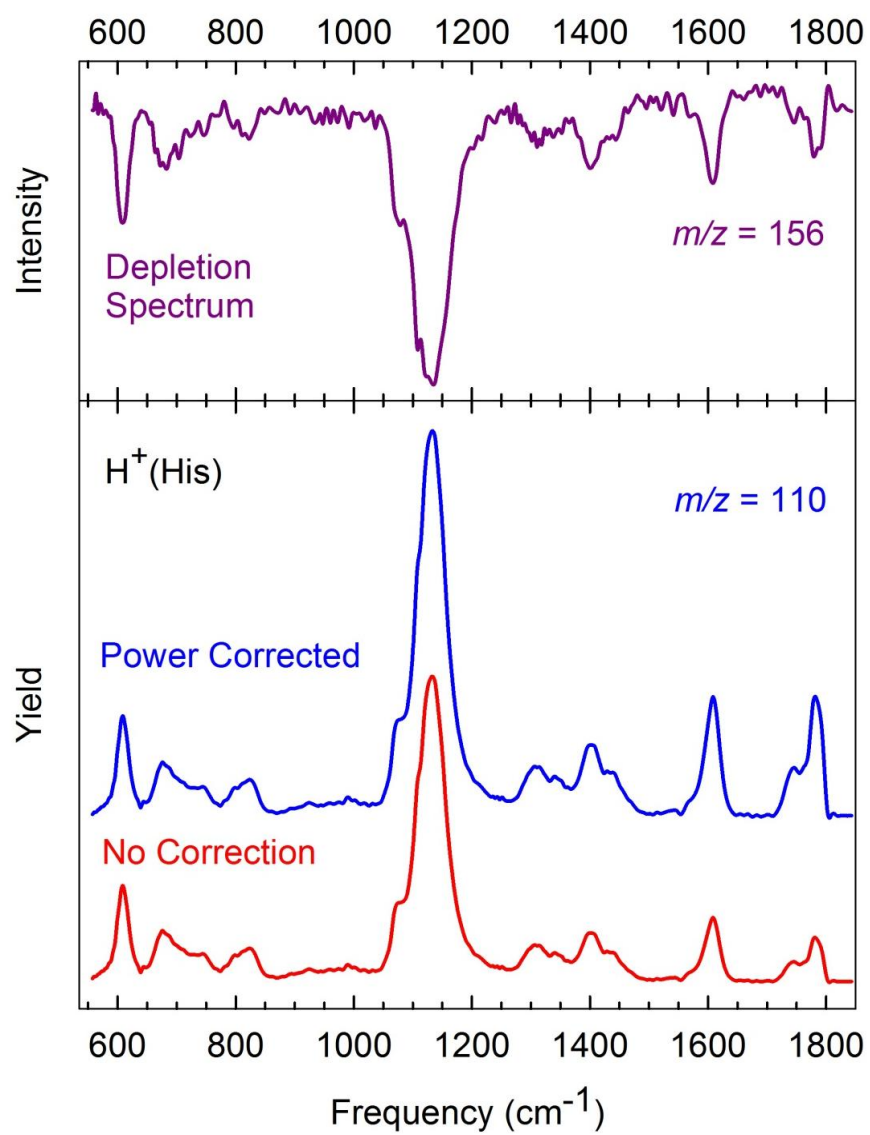


Figure S1

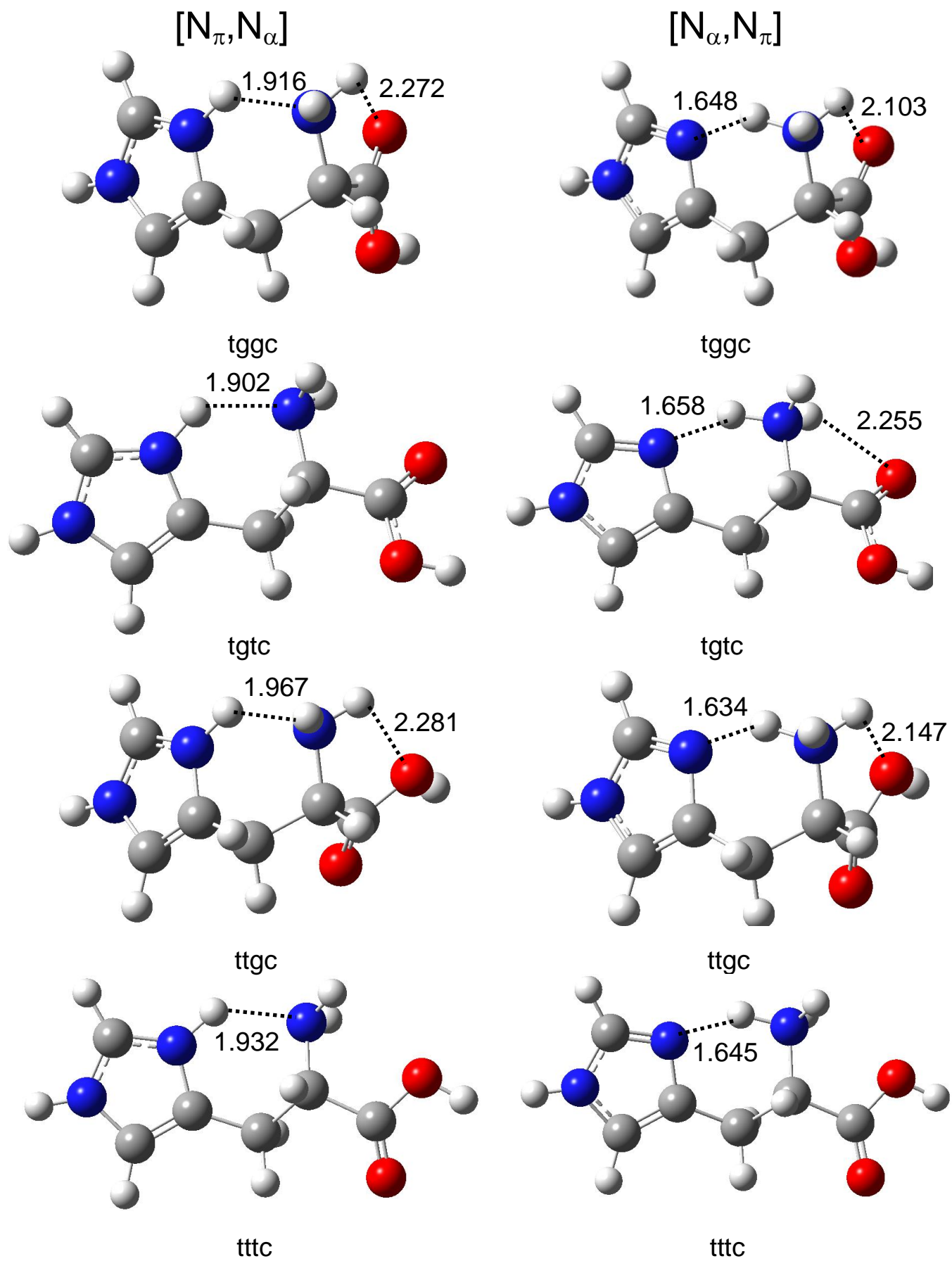
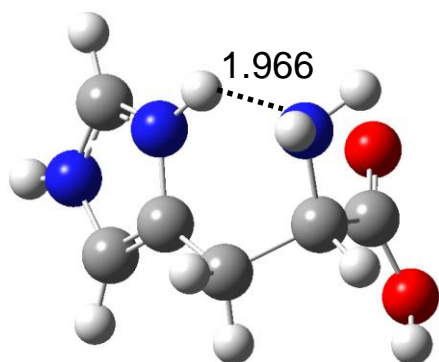
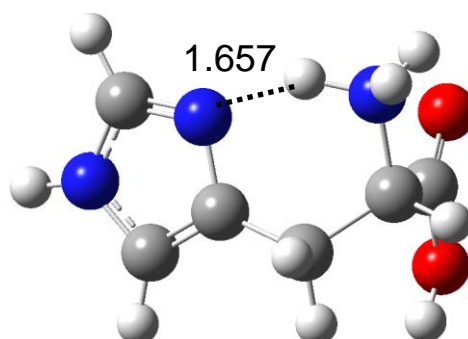


Figure S2

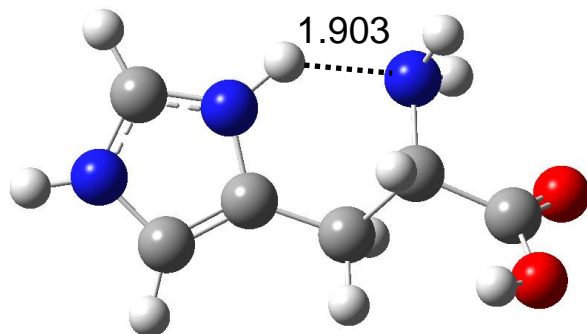
$[N_{\pi}, N_{\alpha}]$



$[N_{\alpha}, N_{\pi}]$

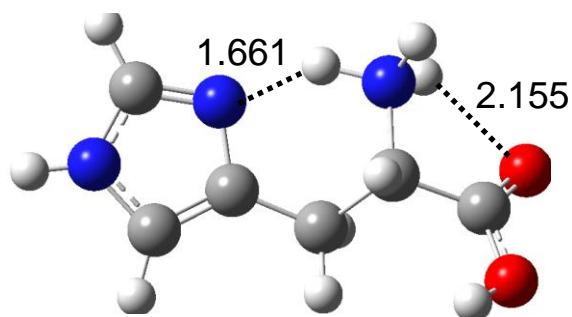


cggc



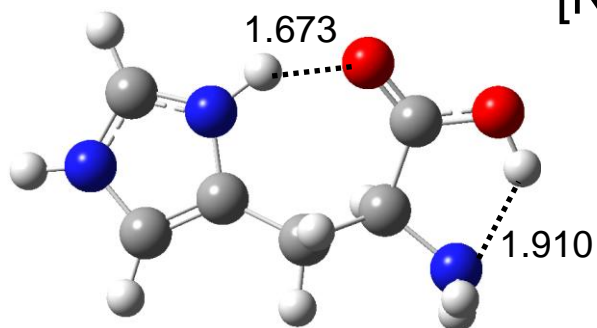
cgtc

cggc

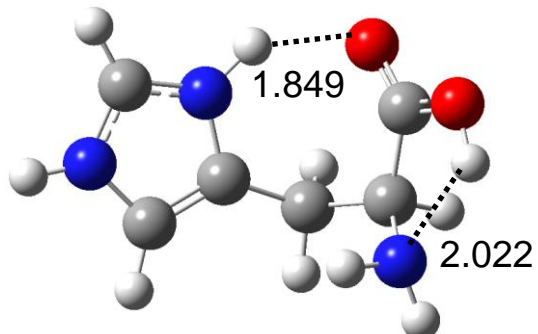


cgtc

$[N_{\pi}, CO]$

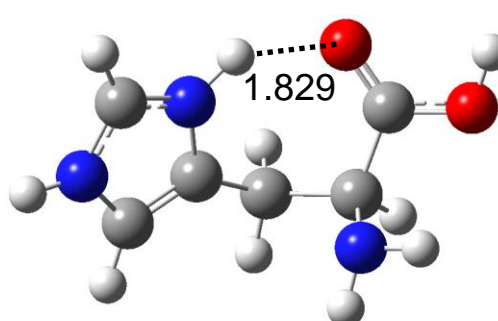


ctg₊g₋



ctg₋g₊

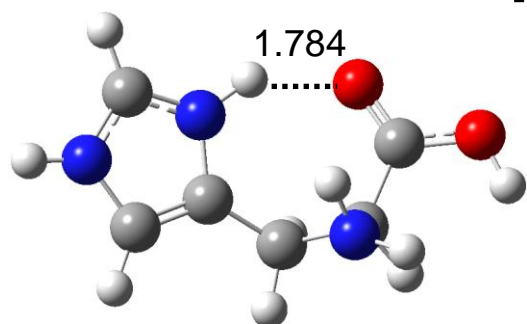
ttg₊g₋(t)



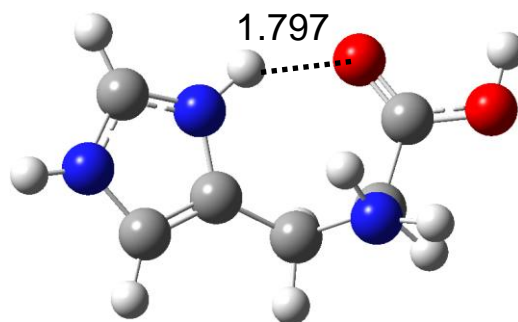
ttg₋g₊(g)

Figure S2

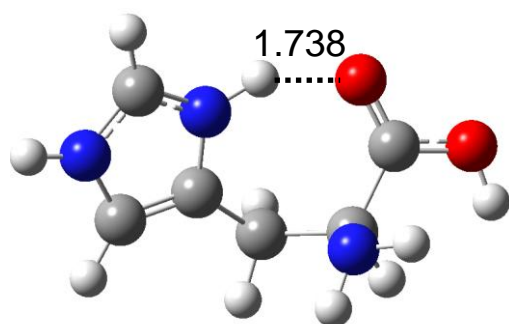
$[N_{\pi}, CO]$



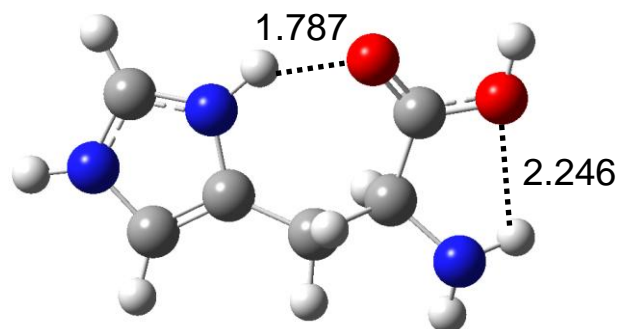
ctg_g+(t)



ttg_g+(t)

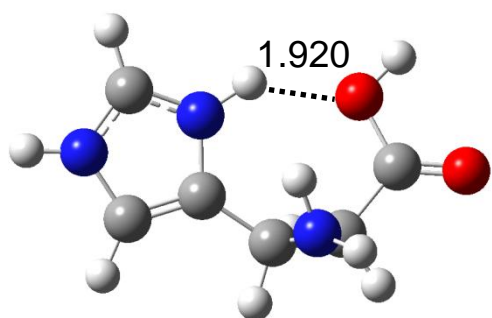


cggg

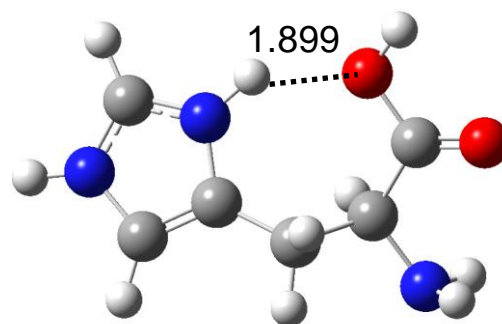


ttg_g-(g)

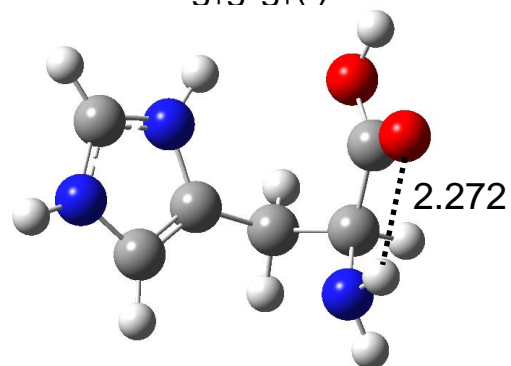
$[N_{\pi}, OH]$



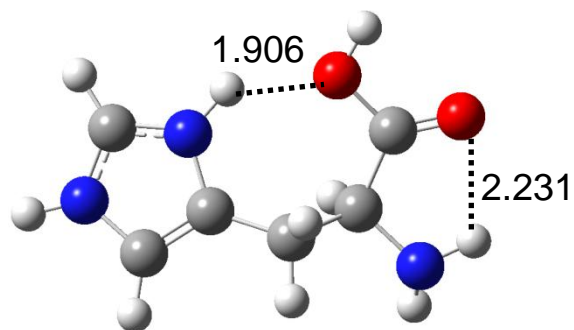
tg_g-g+(t)



tg_g-g-(t)



tcg_g-(g)



tg_g-g-(g)

Figure S2

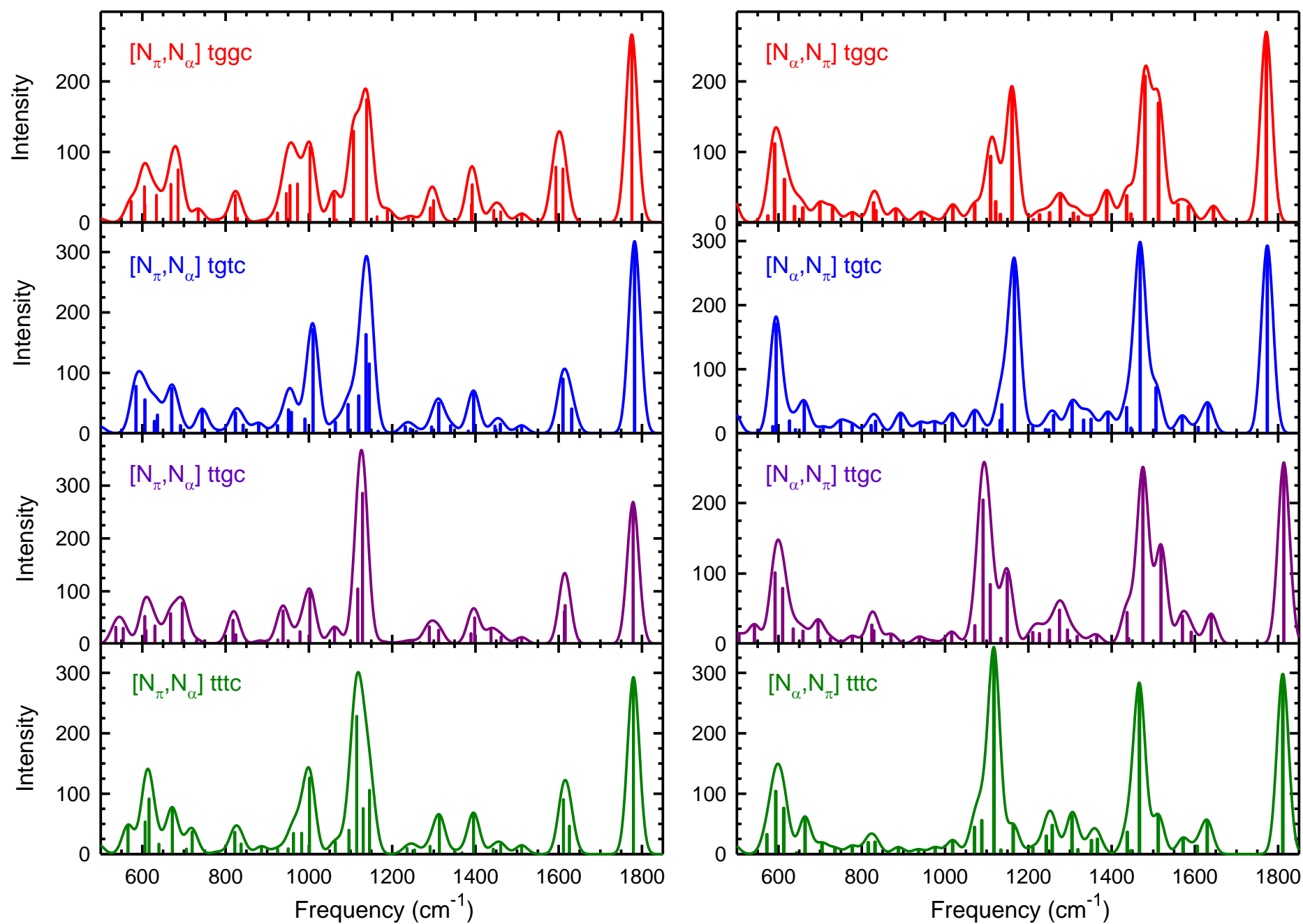


Figure S3

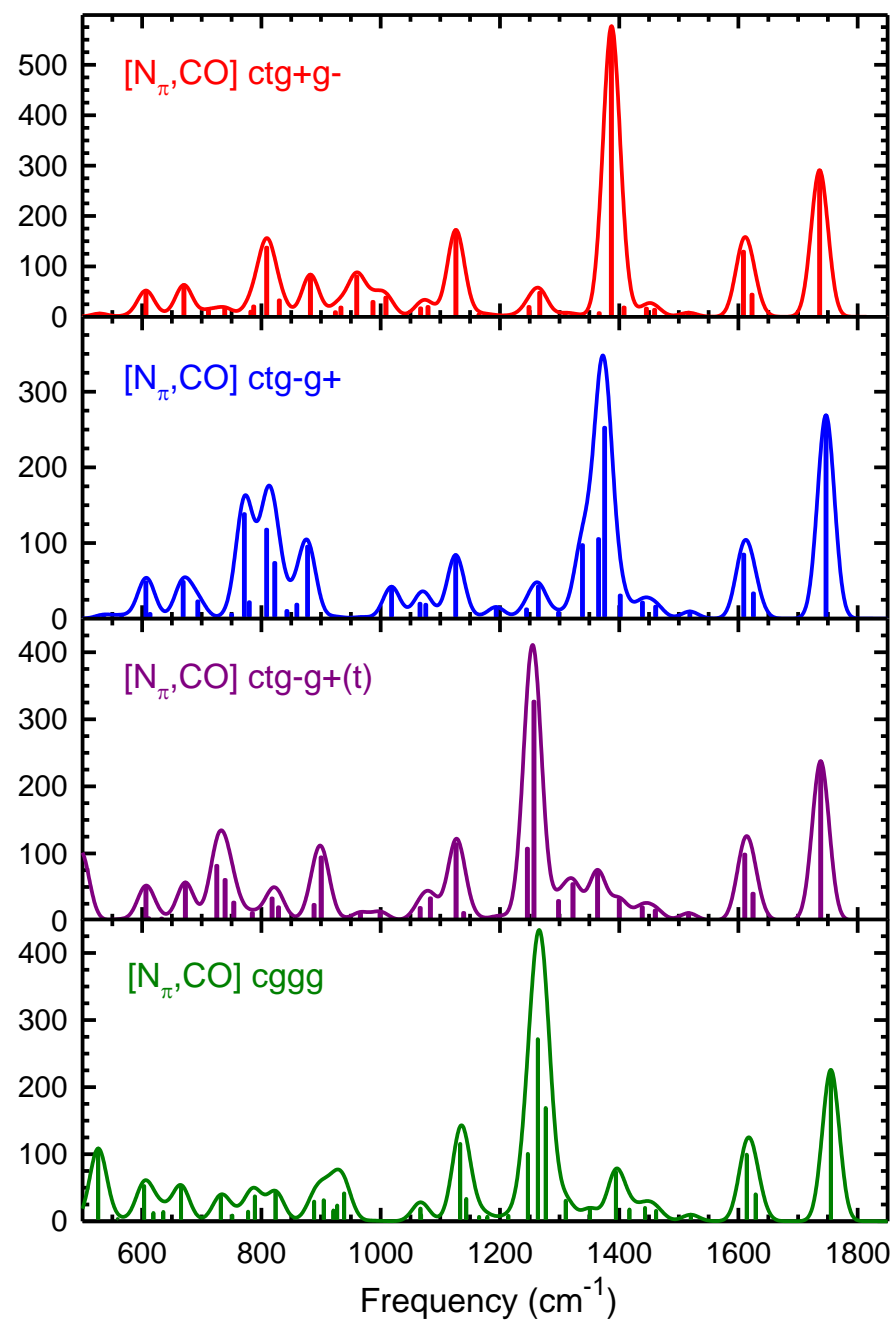
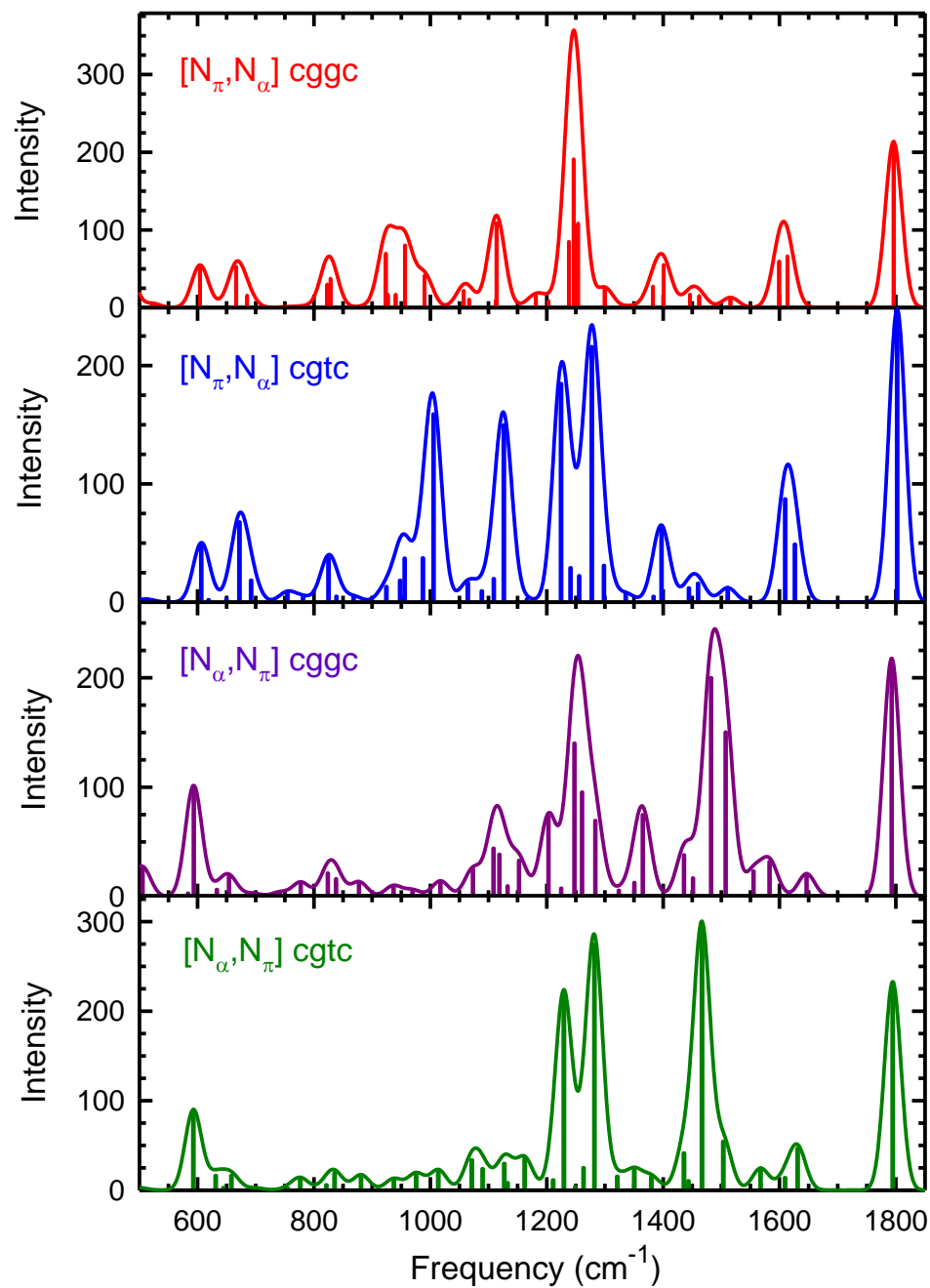


Figure S3

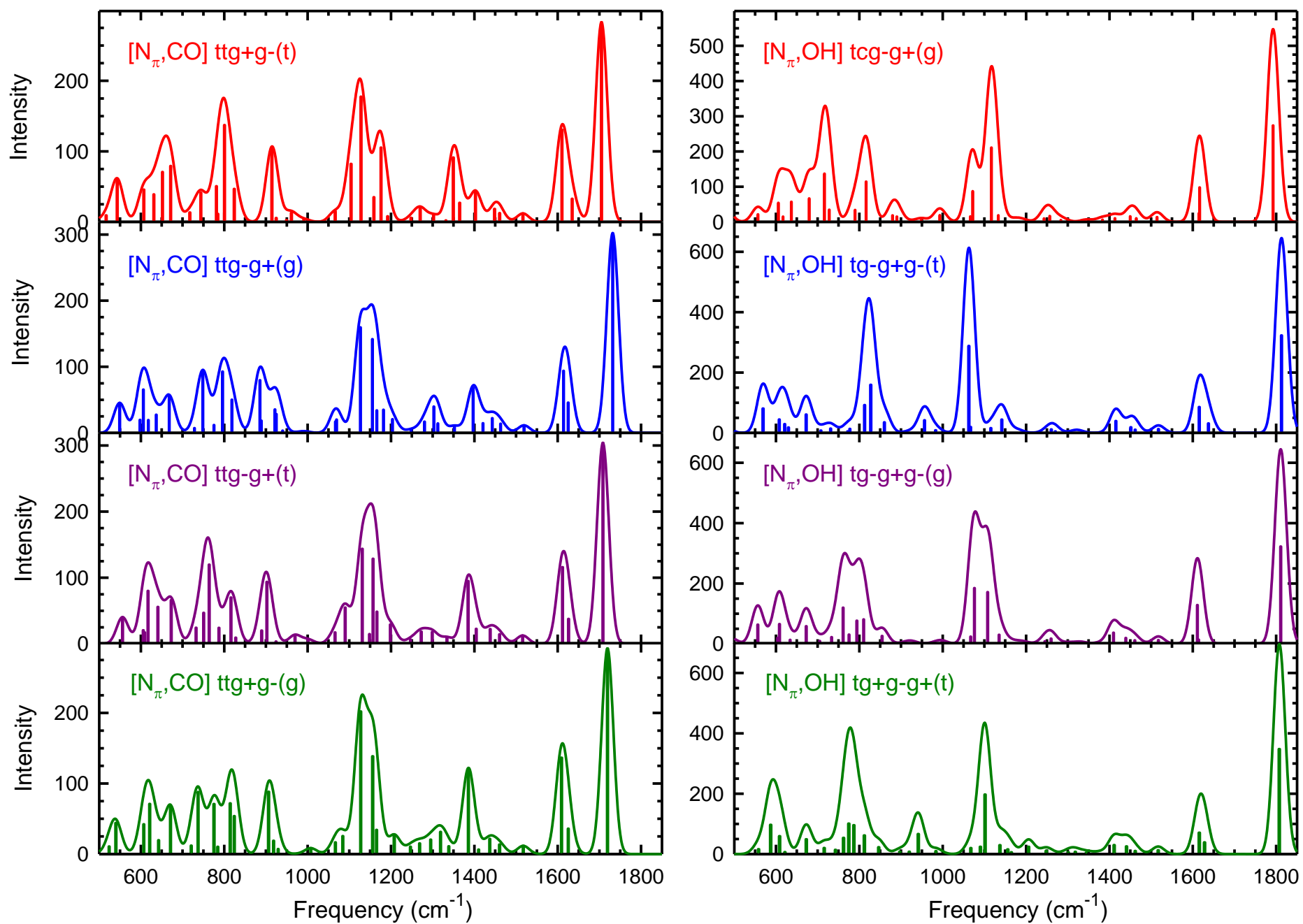


Figure S3

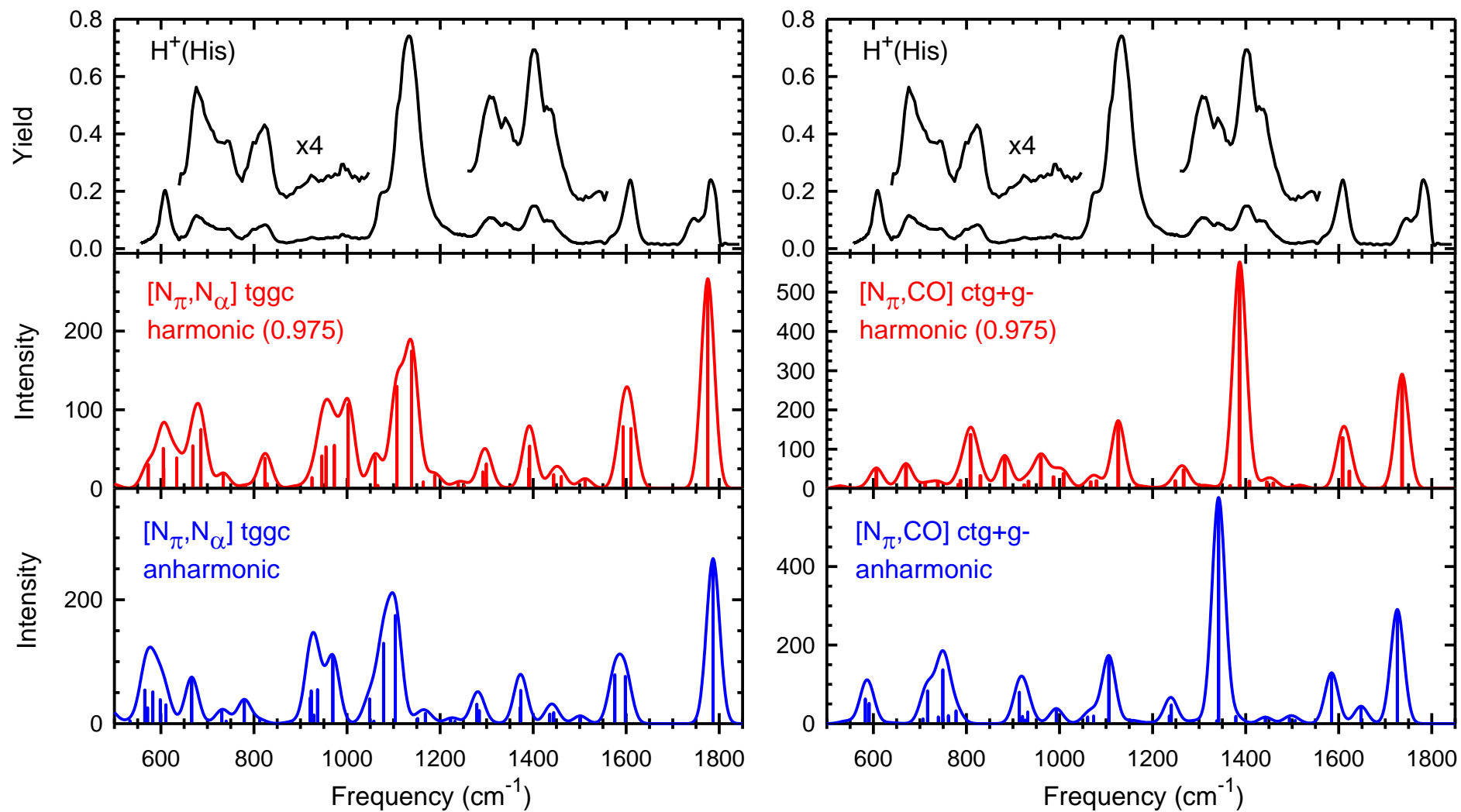


Figure S4

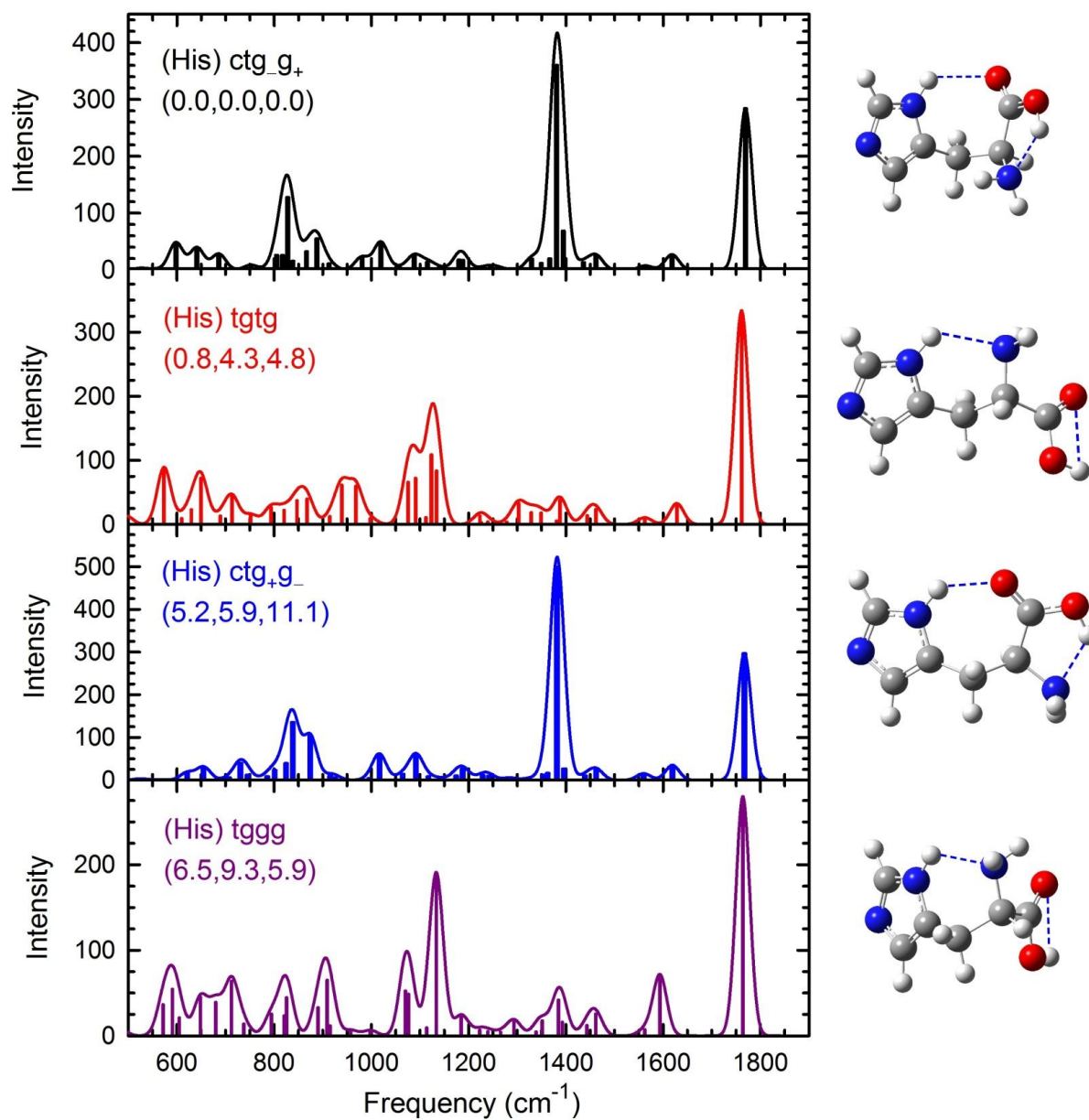


Figure S5

Table S1. Vibrational frequencies (cm^{-1}) scaled by 0.975 and IR intensities (km/mol) for conformers of $\text{H}^+(\text{His})$ calculated at B3LYP/6-311+G(d,p) levels of theory. Bold indicates the region of the IR spectrum included in the present experimental study.

[N $_{\pi}$,N $_{\alpha}$] tggc		[N $_{\pi}$,N $_{\alpha}$] tgtc		[N $_{\pi}$,N $_{\alpha}$] ttgc		[N $_{\pi}$,N $_{\alpha}$] tttc		[N $_{\pi}$,N $_{\alpha}$] cggc		[N $_{\pi}$,N $_{\alpha}$] cgtc	
45	4	45	1	44	3	23	1	51	6	44	4
55	2	66	1	64	6	73	0.6	63	13	67	3
73	1	93	3	76	1	92	2	71	2	97	3
189	28	131	9	188	25	132	5	184	19	129	6
208	6	201	20	216	1	219	27	197	10	194	35
277	6	272	1	281	0	276	6	257	12	269	9
311	7	306	12	307	6	311	4	309	3	308	12
332	15	336	5	338	11	336	6	319	18	339	7
401	3	373	10	397	13	370	12	383	5	383	17
464	18	417	17	418	4	414	7	426	35	411	47
499	5	497	11	536	32	494	16	475	86	456	70
573	31	585	78	554	30	566	48	521	6	512	3
605	51	606	56	606	53	607	54	604	53	606	49
606	26	629	20	609	26	616	92	606	2	619	2
634	39	636	30	630	35	640	17	638	2	650	3
669	54	671	74	668	58	672	76	666	53	672	68
686	75	692	13	696	78	706	9	685	16	692	19
734	19	744	40	730	7	720	37	754	1	754	9
782	4	781	4	779	1	782	4	783	2	781	4
823	39	824	34	818	45	822	36	823	30	825	37
829	6	842	14	825	18	837	17	828	38	839	5
889	3	879	17	882	6	886	13	885	2	868	5

925	14	925	13	925	8	925	9	924	70	924	13
946	41	951	39	938	63	950	9	927	17	948	18
955	53	958	35	951	6	963	35	940	17	956	37
973	55	991	24	979	24	983	35	957	80	987	37
1002	107	1010	172	1002	99	1002	126	990	42	1006	159
1061	40	1064	19	1062	30	1064	21	1057	22	1064	17
1066	4	1094	48	1066	2	1096	40	1067	11	1088	9
1107	130	1120	62	1118	105	1115	228	1113	10	1109	20
1139	175	1137	164	1129	286	1130	76	1114	109	1126	150
1164	8	1145	115	1163	1	1146	106	1163	2	1141	1
1188	17	1166	4	1179	4	1165	0.2	1181	15	1166	3
1205	2	1232	11	1215	3	1236	10	1203	9	1225	185
1239	6	1244	7	1243	6	1252	4	1238	85	1241	29
1252	4	1258	3	1267	3	1254	7	1246	191	1256	22
1292	21	1295	11	1289	33	1291	13	1254	108	1277	216
1299	31	1312	50	1312	26	1313	62	1300	26	1298	31
1341	1	1340	13	1341	0	1351	4	1343	2	1336	7
1391	26	1383	4	1389	20	1368	3	1383	27	1384	5
1392	54	1396	68	1398	50	1396	68	1401	55	1397	62
1444	18	1447	12	1437	26	1443	9	1446	17	1444	12
1461	15	1460	15	1462	14	1461	16	1462	15	1460	16
1512	12	1511	13	1511	13	1511	15	1516	13	1511	12
1593	79	1610	90	1614	61	1611	91	1599	60	1610	87
1610	76	1631	41	1616	73	1626	47	1614	66	1626	49
1775	266	1782	318	1779	269	1779	293	1796	214	1802	248
2946	11	2953	1	2926	14	2950	1	2928	26	2957	1
2967	4	2995	4	2966	4	2965	6	2967	5	2975	12

3044	0.1	3037	0	3043	0	3047	1	3022	3	3021	2
3085	731	3067	796	3158	626	3110	760	3171	625	3072	786
3202	42	3201	42	3204	43	3201	42	3202	45	3201	43
3205	8	3205	8	3208	7	3205	8	3206	4	3204	8
3400	20	3383	20	3403	14	3395	13	3410	16	3368	26
3478	33	3452	25	3469	28	3465	24	3484	27	3448	26
3531	185	3529	191	3531	184	3529	190	3531	189	3527	193
3649	126	3641	128	3648	127	3647	137	3699	71	3707	64

[N _α ,N _π] tggc		[N _α ,N _π] tgtc		[N _α ,N _π] ttgc		[N _α ,N _π] ttcc		[N _α ,N _π] cggc		[N _α ,N _π] cgtc	
55	1	58	1	49	2	28	0	50	4	60	2
61	4	63	5	63	3	75	9	60	9	69	8
82	5	91	14	73	10	85	9	84	6	96	19
207	15	146	6	214	7	148	16	206	22	145	19
223	46	213	15	226	54	223	13	227	53	210	16
286	10	278	23	291	1	280	16	298	26	280	40
329	57	313	15	329	50	306	14	329	38	318	18
342	19	338	80	349	25	343	85	343	36	342	86
411	5	383	7	420	3	395	1	408	48	385	20
465	22	402	43	457	30	415	22	432	57	402	9
488	38	494	32	505	14	491	16	480	7	449	115
574	10	586	11	542	28	572	33	505	26	499	3
591	112	594	171	592	101	593	104	584	3	593	90
614	62	626	20	610	79	613	76	594	99	631	16
638	23	641	6	636	22	643	3	633	7	644	3
659	21	662	48	659	19	664	61	654	18	658	17

699	27	707	10	695	33	705	18	695	3	700	3
730	21	749	19	725	8	736	10	742	4	755	2
777	14	777	13	777	12	777	14	777	13	776	14
829	28	823	13	824	27	816	20	824	22	821	6
834	17	833	19	829	19	832	20	838	16	835	19
882	20	893	32	870	14	888	12	878	13	881	17
935	2	935	1	935	2	932	2	934	1	934	1
943	13	941	16	938	8	937	6	937	9	937	12
970	5	975	18	971	4	976	11	969	6	976	19
1019	25	1017	31	1016	17	1018	23	1017	14	1014	23
1071	26	1071	34	1072	27	1071	45	1073	25	1071	34
1110	94	1091	7	1091	205	1088	56	1109	44	1090	24
1122	30	1132	21	1109	85	1117	332	1119	39	1127	30
1133	12	1136	45	1134	8	1134	7	1133	10	1133	8
1161	191	1166	268	1149	101	1164	48	1152	33	1162	36
1212	4	1211	10	1211	17	1211	11	1203	73	1211	11
1227	11	1241	6	1227	15	1243	31	1225	8	1229	216
1251	14	1248	5	1251	20	1249	2	1248	140	1249	4
1277	38	1261	28	1275	49	1257	48	1261	95	1263	25
1308	14	1305	48	1294	20	1305	64	1284	70	1282	275
1320	8	1333	21	1317	11	1319	8	1324	6	1321	15
1351	8	1351	22	1351	4	1352	23	1351	13	1351	22
1388	45	1391	33	1364	11	1366	25	1365	75	1380	15
1436	38	1436	41	1437	45	1438	37	1436	38	1436	41
1447	12	1446	9	1441	8	1447	6	1451	17	1444	10
1480	208	1469	291	1475	248	1467	277	1482	200	1467	292
1513	170	1507	71	1519	139	1512	65	1507	150	1503	55

1559	26	1570	28	1570	40	1572	27	1555	23	1568	24
1585	23	1608	10	1591	17	1606	14	1583	32	1610	14
1645	23	1631	46	1639	43	1630	54	1646	21	1631	47
1771	270	1774	293	1814	257	1811	298	1793	218	1795	233
2394	1309	2446	1347	2338	1295	2384	1369	2423	1279	2466	1317
2955	11	2944	8	2954	12	2939	11	2954	10	2949	5
3001	2	3024	0	2997	2	3005	0	2991	2	3005	1
3041	0	3036	0	3040	0	3040	1	3008	6	3021	2
3185	7	3184	7	3184	7	3185	7	3185	8	3184	8
3195	5	3194	5	3197	6	3195	6	3194	5	3193	5
3290	99	3324	95	3355	79	3367	73	3260	114	3292	113
3427	92	3409	77	3423	82	3425	72	3424	93	3405	79
3543	142	3541	147	3543	143	3541	148	3540	147	3540	149
3638	156	3635	169	3642	157	3636	164	3706	71	3696	82

[N _π ,CO] ctg ₊ g ₋		[N _π ,CO] ctg ₋ g ₊		[N _π ,CO] ctg ₋ g ₊ (t)		[N _π ,CO] cggg		[N _π ,CO] ttg ₊ g ₋ (t)		[N _π ,CO] ttg ₋ g ₊ (g)	
58	1	61	0	30	3	24	1	28	2	33	1
89	6	81	5	85	7	93	9	85	4	84	7
119	2	100	1	96	1	102	1	104	0	101	1
156	29	171	25	152	14	161	25	156	16	157	19
247	26	226	25	201	29	206	3	215	28	214	7
291	11	269	11	217	43	234	40	239	12	248	25
313	7	308	7	267	8	276	17	286	7	266	4
324	3	337	14	278	26	290	14	310	4	293	15
353	19	368	7	326	4	331	6	339	15	335	2
376	13	437	4	362	3	342	5	352	7	365	8

529	6	536	5	497	103	526	108	517	9	549	45
578	2	566	4	564	2	559	3	543	60	598	20
606	52	606	48	606	48	603	53	607	46	606	65
639	2	613	6	611	3	619	12	631	39	618	19
670	63	669	49	633	3	636	14	652	71	637	27
711	12	693	23	673	56	665	52	671	79	668	55
738	17	750	5	725	82	732	36	717	13	729	7
782	10	771	138	739	60	751	8	744	41	749	90
787	21	780	22	754	27	778	14	781	51	775	12
809	137	809	118	785	11	789	37	785	11	796	93
830	33	822	74	818	33	824	43	801	137	818	50
882	83	843	10	829	20	888	29	824	47	886	80
924	9	860	18	888	23	905	31	914	103	889	19
933	18	877	95	900	94	921	16	925	6	922	35
960	80	923	3	924	2	927	23	949	3	925	28
987	30	969	2	966	12	939	41	961	13	940	3
1009	38	1018	42	999	13	987	1	991	4	990	3
1067	17	1066	20	1066	19	1067	19	1066	15	1067	17
1079	20	1076	18	1083	33	1068	9	1104	82	1069	20
1126	172	1126	84	1126	114	1133	115	1128	177	1127	160
1150	2	1141	0	1139	11	1144	33	1159	35	1155	142
1165	4	1163	2	1148	0	1165	7	1165	0	1166	34
1185	3	1194	15	1163	3	1179	7	1176	105	1182	35
1217	2	1198	0	1199	7	1214	8	1192	8	1203	21
1249	20	1245	12	1246	107	1247	101	1248	6	1248	5
1267	48	1264	43	1257	326	1264	272	1270	19	1280	17
1309	7	1298	8	1298	29	1277	169	1302	9	1303	40

1329	3	1338	97	1323	54	1310	30	1332	2	1312	14
1367	7	1365	105	1360	2	1351	19	1350	91	1352	10
1387	568	1376	252	1364	72	1395	73	1365	27	1397	68
1408	19	1402	31	1400	31	1417	17	1403	44	1421	15
1446	16	1439	21	1439	20	1443	20	1448	18	1443	22
1459	14	1461	16	1461	15	1462	16	1461	12	1463	14
1516	8	1518	9	1516	11	1520	10	1517	12	1519	11
1608	129	1609	85	1611	98	1614	99	1610	131	1614	94
1623	44	1625	33	1624	40	1629	40	1635	33	1625	46
1736	291	1747	269	1738	237	1755	226	1705	283	1732	302
2957	1	2966	3	2970	2	2880	53	2945	4	2909	22
2973	5	2983	1	2978	11	2970	3	2966	5	2978	3
3002	1079	3029	2	3034	1	3013	2	3040	1	3018	2
3021	3	3199	44	3200	58	3136	894	3196	670	3202	39
3199	41	3204	14	3207	75	3201	41	3201	154	3206	13
3203	8	3269	507	3212	623	3205	6	3205	6	3271	622
3346	309	3427	43	3438	13	3414	12	3428	15	3413	11
3428	9	3451	189	3521	16	3488	13	3508	19	3484	14
3514	28	3514	24	3529	185	3533	183	3529	186	3532	181
3529	186	3528	189	3703	92	3701	96	3634	134	3636	130

[N _π ,CO] ttg _{-g⁺} (t)		[N _π ,CO] ttg _{+g⁻} (g)		[N _π ,OH] tcg _{-g⁺} (g)		[N _π ,OH] tg _{-g⁺g⁻} (t)		[N _π ,OH] tg _{-g⁺g⁻} (g)		[N _π ,OH] tg _{+g⁻g⁺} (t)	
40	2	42	1	17	1	42	1	43	2	23	1
87	4	88	4	57	5	70	0	70	0	64	0
100	0	108	0	85	2	94	3	92	1	84	3
151	13	158	15	110	8	143	12	145	12	138	11

210	3	231	17	213	1	185	35	178	30	200	1
245	33	244	21	240	31	219	4	224	3	238	31
272	15	296	5	278	3	269	3	287	5	263	9
278	14	326	2	302	2	297	9	321	7	273	21
327	7	330	4	376	1	347	18	333	3	334	2
361	7	362	23	461	11	365	7	371	15	352	10
556	40	524	11	480	20	476	17	492	10	558	16
606	21	540	44	557	21	569	81	556	64	587	97
609	17	607	42	606	54	608	44	604	20	604	1
617	80	621	71	617	15	621	29	608	65	609	59
641	56	642	20	637	57	630	18	634	13	622	7
673	66	671	67	663	3	672	61	673	58	673	49
732	24	721	12	680	67	708	8	705	9	716	20
751	47	737	88	716	137	731	14	734	22	743	14
764	120	775	71	728	35	772	5	761	120	762	54
787	24	785	10	790	34	777	13	775	31	775	101
816	70	814	72	816	114	813	92	794	77	787	96
828	9	824	54	827	2	827	159	810	81	812	62
890	20	906	88	880	18	860	35	855	26	846	23
902	94	918	19	890	15	922	3	912	3	897	8
924	3	929	7	919	1	941	1	926	4	920	8
970	13	982	1	949	5	956	42	979	2	941	66
1001	7	1008	8	993	19	983	9	997	5	984	10
1066	17	1067	17	1066	16	1063	288	1067	24	1067	20
1090	55	1084	26	1072	87	1067	19	1076	185	1090	24
1131	144	1127	202	1117	211	1115	16	1108	171	1102	197
1148	15	1156	138	1133	19	1142	44	1135	30	1137	29

1157	129	1165	34	1163	2	1165	1	1162	2	1156	15
1166	49	1176	1	1176	3	1176	4	1168	3	1165	6
1199	29	1208	27	1190	3	1182	2	1192	4	1206	24
1247	7	1247	10	1243	10	1245	2	1245	8	1248	11
1273	19	1269	15	1257	17	1261	11	1260	17	1273	1
1299	18	1295	20	1283	5	1270	5	1280	1	1301	6
1334	10	1319	31	1294	1	1318	3	1302	3	1318	7
1366	1	1339	11	1345	4	1326	2	1331	4	1344	5
1385	95	1386	121	1383	6	1377	0	1378	2	1376	4
1405	23	1410	6	1413	10	1415	39	1410	37	1411	30
1438	22	1437	21	1450	16	1451	18	1439	19	1441	25
1461	14	1461	14	1464	10	1462	11	1461	12	1462	10
1516	13	1517	12	1514	14	1518	12	1517	12	1517	13
1611	116	1609	137	1615	25	1615	86	1611	128	1616	71
1626	38	1625	36	1616	98	1638	31	1614	14	1628	39
1708	304	1719	291	1793	274	1813	323	1811	322	1808	348
2969	3	2843	33	2896	18	2961	1	2872	27	2968	3
3012	2	2982	1	2997	3	2974	8	2979	1	3024	1
3035	0	3028	1	3039	1	3036	1	3037	1	3032	1
3200	65	3200	43	3203	44	3201	45	3201	44	3201	43
3206	114	3205	29	3215	17	3206	14	3205	13	3207	15
3211	589	3221	711	3425	19	3347	538	3374	497	3372	483
3431	13	3439	16	3499	195	3421	17	3438	26	3430	13
3513	17	3517	22	3501	37	3495	19	3522	31	3508	16
3529	185	3529	186	3527	158	3526	191	3527	189	3526	187
3633	128	3638	141	3639	116	3631	114	3636	132	3632	119